# RESEARCH ARTICLE



WILEY

# Extending CAS elements to remove shear and membrane locking from quadratic NURBS-based discretizations of linear plane Timoshenko rods

# Mahmoud Golestanian | Hugo Casquero

Department of Mechanical Engineering, University of Michigan - Dearborn, Dearborn, Michigan, USA

#### Correspondence

Hugo Casquero, Department of Mechanical Engineering, University of Michigan - Dearborn, 4901 Evergreen Road, Dearborn, MI, 48128-1491, USA. Email: casquero@umich.edu

## **Funding information**

Ansys; Honda; National Science Foundation, Grant/Award Number: CMMI-2138187

## **Abstract**

Continuous-assumed-strain (CAS) elements were recently introduced (Casquero and Golestanian. Comput Methods Appl Mech Eng. 2022; 399:115354.) to remove the membrane locking present in quadratic C<sup>1</sup>-continuous NURBS-based discretizations of linear plane curved Kirchhoff rods. In this work, we generalize CAS elements to remove shear and membrane locking from quadratic NURBS-based discretizations of linear plane curved Timoshenko rods. CAS elements are an assumed strain treatment that interpolates the shear and membrane strains at the knots using linear Lagrange polynomials. Consequently, the inter-element continuity of the shear and membrane strains is maintained. The numerical experiments considered in this work show that CAS elements excise the spurious oscillations in shear and membrane forces caused by shear and membrane locking. Furthermore, when using CAS elements with either full or reduced integration, the convergence of displacements, rotations, and stress resultants is independent of the slenderness ratio up to 10<sup>4</sup> while the convergence is highly dependent on the slenderness ratio when using NURBS elements. We apply the locking treatment of CAS elements to quadratic  $C^0$ -continuous NURBS and the resulting element type is named discontinuous-assumed-strain (DAS) elements. Comparisons among CAS and DAS elements show that once locking is properly removed,  $C^1$  continuity across element boundaries results in higher accuracy than  $C^0$  continuity across element boundaries. Lastly, CAS elements result in a simple numerical scheme that does not add any significant computational burden in comparison with the locking-prone NURBS-based discretization of the Galerkin method.

# KEYWORDS

assumed natural strain, convergence studies, isogeometric analysis, membrane locking, shear locking, Timoshenko rods

This is an open access article under the terms of the Creative Commons Attribution License, which permits use, distribution and reproduction in any medium, provided the original work is properly cited.

© 2023 The Authors. International Journal for Numerical Methods in Engineering published by John Wiley & Sons Ltd.

# 1 | INTRODUCTION

Isogeometric analysis (IGA)<sup>1,2</sup> makes possible the design and analysis of rods<sup>3-8</sup> and shells<sup>9-18</sup> using the same geometric representation in computer-aided-design (CAD) and finite-element-analysis (FEA) programs. This is accomplished by using the same spline-based representations of the geometry in CAD and FEA programs. However, when applied to structural theories that take into account transverse shear deformations, spline-based discretizations suffer from the same types of locking as conventional FEA discretizations based on Lagrange polynomials.<sup>19-21</sup> Thus, spline-based discretizations of curved Timoshenko rods<sup>22-26</sup> and Reissner–Mindlin shells<sup>27-31</sup> are adversely affected by shear and membrane locking. Shear and membrane locking lead to displacements, rotations, and bending moments with smaller values than expected and shear and membrane forces with large-amplitude spurious oscillations.

Several numerical schemes have been developed to overcome locking in conventional FEA discretizations based on Lagrange polynomials with  $C^0$  continuity across element boundaries, such as reduced integration,  $^{32-35}$  selective reduced integration, 36-38 assumed strain treatments, 39-42 and mixed formulations. 43-45 Due to the higher inter-element continuity of splines, a direct deployment of the numerical schemes mentioned above is not an effective strategy to overcome locking. Reduced/selective-reduced integration rules at the element level and assumed strain treatments with discontinuous strain across elements boundaries fail to properly vanquish locking<sup>46-50</sup> while the condensation of strain variables at the element level cannot be carried out in Bubnov-Galerkin discretizations of mixed formulations. 6,19 Thus, the higher inter-element continuity of splines demands to develop new numerical schemes to overcome locking. Reduced/selective-reduced integration rules at the patch level are explored in References 51-53. In Reference 54, a Petrov-Galerkin discretization of a mixed formulation that condenses the strain variables at the element level by leveraging Bézier dual basis functions<sup>55,56</sup> is proposed. Global versions of the  $\overline{B}$  method<sup>57</sup> have been developed for nearly incompressible solids, 58 Timoshenko rods, 22,26 Kirchhoff rods, 46 Kirchhoff-Love shells, 47 and solid shells. 48 Analogously, global versions of the discrete strain gap (DSG) method<sup>59,60</sup> have been developed for Timoshenko rods<sup>19,22</sup> and Kirchhoff-Love, Reissner-Mindlin, and 7-parameter shells.<sup>27</sup> These global versions of the  $\overline{B}$  and DSG methods successfully remove locking by constructing assumed strains that preserve the inter-element continuity of the compatible strains. Nevertheless, as mentioned by the authors, <sup>22,46-48</sup> these numerical schemes are hampered by computing the inverse of a global Gram matrix and having a global stiffness matrix that is not a sparse matrix. In order to increase the computational efficiency of the global  $\overline{B}$  method, assumed strains that preserve the inter-element continuity of the compatible strains are reconstructed from B projections at the element level in References 46 and 47. Although the global stiffness matrix is no longer a full matrix, its bandwidth is still larger than the bandwidth of the global stiffness matrix obtained by applying the locking-prone NURBS-based discretization of the Galerkin method. Solving systems of linear algebraic equations at the element level and performing matrix multiplications to obtain the stiffness matrix are also needed. In Reference 50, the membrane locking present in  $C^1$ -continuous quadratic NURBS-based discretizations of linear plane Kirchhoff rods is overcame constructing continuous assumed strains through the linear interpolation of the compatible strains at the knots. The resulting element type is named continuous-assumed-strain (CAS) elements. To the authors' knowledge, CAS elements are the only element type based on quadratic NURBS which has shown to effectively remove membrane locking for an ample range of slenderness ratios while having the following distinctive characteristics: (1) no additional degrees of freedom are added, (2) no additional systems of algebraic equations need to be solved, (3) no matrix multiplications are needed to obtain the stiffness matrix, and (4) the nonzero pattern of the stiffness matrix is preserved. Coming up with a locking treatment for cubic NURBS that effectively removes membrane locking for an ample range of slenderness ratios while having the four distinctive characteristics mentioned above remains an open problem.

In this work, we extend CAS elements to remove shear and membrane locking from quadratic NURBS-based discretizations of linear plane curved Timoshenko rods. In order to do so, CAS elements interpolate the shear and membrane strains at the knots using linear Lagrange polynomials. Thus, the inter-element continuity of the shear and membrane assumed strains is the same as that of the compatible strains. In addition, we apply the same assumed strain treatment to quadratic  $C^0$ -continuous NURBS and the resulting element type is named discontinuous-assumed-strain (DAS) elements. This is done to show that once locking is properly removed,  $C^1$  continuity across element boundaries results in higher accuracy than  $C^0$  continuity across element boundaries. Shear and membrane locking cause displacements, rotations, and bending moments with smaller values than expected and shear and membrane forces with large-amplitude spurious oscillations. Therefore, we study the convergence and plot the distributions of displacements, rotations, and stress resultants so as to show that CAS elements successfully vanquish shear and membrane locking.

The article is outlined as follows. Section 2 describes the mathematical theory of linear plane curved Timoshenko rods. Section 3 summarizes how to solve the problem using a NURBS-based discretization of the Galerkin method. Section 4 extends CAS elements to treat both the membrane locking and the shear locking existent in quadratic NURBS-based discretizations of linear plane Timoshenko rods. In Section 5, the performance of CAS elements with full and reduced integration is evaluated using exact solutions and comparisons with the NURBS-based discretization of the Galerkin method. Sections 5.1-5.3 consider a clamped quarter-circular arc with a moment applied at the free end, a clamped-clamped semi-circular arch under a distributed load, and a simply-supported straight rod under a distributed load, respectively. In Section 6, concluding remarks and directions of future work are drawn.

#### 2 LINEAR PLANE CURVED TIMOSHENKO ROD MODEL

In this section, we describe Timoshenko rods without considering material or geometrical nonlinearities, that is, infinitesimal deformations and small strains are assumed. The geometry of the rod is defined by the axis of the rod and its cross section.

#### Kinematics in infinitesimal deformations 2.1

The position vector of a material point on the axis of the rod is defined by the parametric curve  $\mathbf{r}(\xi)$ :  $[0,1] \mapsto \mathbb{R}^2$  in which  $\xi$  is the parametric coordinate. For convenience, we reparametrize the axis of the rod in terms of its arc length s, which is achieved taking into account that

$$ds = \left\| \frac{d\mathbf{r}}{d\xi} \right\| d\xi,\tag{1}$$

where  $\|\cdot\|$  denotes the length of a vector. The length of the rod is defined as

$$L = \int_{0}^{1} \left\| \frac{\mathrm{d}\mathbf{r}}{\mathrm{d}\xi} \right\| d\xi. \tag{2}$$

The tangential and normal displacements of a material point on the axis of the rod are defined by  $u(s):[0,L]\mapsto\mathbb{R}$ and  $v(s): [0,L] \mapsto \mathbb{R}$ , respectively. The in-plane rotation of the cross section is defined as  $\theta(s): [0,L] \mapsto \mathbb{R}$ . The positive signs of  $u, v, \theta$  are indicated in Figure 1.

The membrane strain is defined as

$$\epsilon = \frac{du}{ds} - \frac{v}{R},\tag{3}$$

where *R* is the radius of curvature of the rod axis. The shear strain is defined as

$$\gamma = \frac{u}{R} + \frac{dv}{ds} - \theta. \tag{4}$$

The bending strain is defined as

$$\kappa = \frac{d\theta}{ds}.\tag{5}$$

#### 2.2 Linear material

The stress resultants of plane curved Timoshenko rods are the membrane force, the shear force, and the bending moment. For a linear material, the membrane force is defined as

$$\mathcal{N} = EA\epsilon, \tag{6}$$

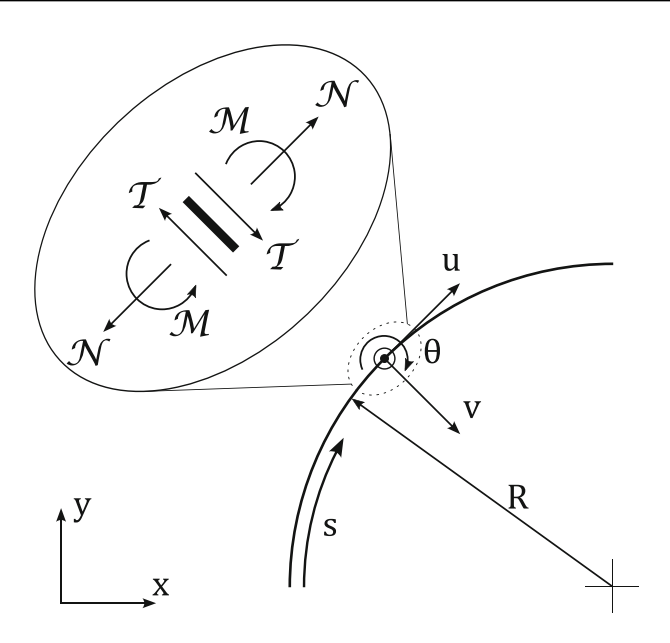


FIGURE 1 Positive signs for the tangential displacement u, the normal displacement v, the rotation  $\theta$ , the membrane force  $\mathcal{N}$ , the shear force  $\mathcal{T}$ , and the bending moment  $\mathcal{M}$ .

where E is the Young modulus and A is the area of the cross section. The shear force is defined as

$$\mathcal{T} = \mu A \gamma, \tag{7}$$

where  $\mu = \frac{E}{2(1+v)}$  is the shear modulus and v is the Poisson ratio. The bending moment is defined as

$$\mathcal{M} = EI\kappa, \tag{8}$$

where I is the cross section's moment of inertia. The positive signs of  $\mathcal{N}, \mathcal{T}, \mathcal{M}$  are indicated in Figure 1.

#### 2.3 Variational form

The principle of virtual work states that the internal virtual work ( $\delta W^{int}$ ) must be equal to the external virtual work  $(\delta W^{ext})$  for any virtual displacements and rotations  $(\delta u, \delta v, \delta \theta)$ , that is,

$$\delta W^{int} = \delta W^{ext} \quad \forall (\delta u, \delta v, \delta \theta), \tag{9}$$

with

$$\delta W^{int} = \int_{0}^{L} \left( \mathcal{N} \delta \epsilon + \mathcal{T} \delta \gamma + \mathcal{M} \delta \kappa \right) \mathrm{d}s, \tag{10}$$

$$\delta W^{int} = \int_{0}^{L} \left( \mathcal{N} \delta \epsilon + \mathcal{T} \delta \gamma + \mathcal{M} \delta \kappa \right) ds, \tag{10}$$

$$\delta W^{ext} = \int_{0}^{L} \left( f_t \delta u + f_n \delta v + m \delta \theta \right) ds + N_0 \delta u(0) + T_0 \delta v(0) + M_0 \delta \theta(0) \tag{11}$$

$$+ N_L \delta u(L) + T_L \delta v(L) + M_L \delta \theta(L),$$

where  $\delta\epsilon$ ,  $\delta\gamma$ , and  $\delta\kappa$  are the virtual membrane strain, the virtual shear strain, and the virtual bending strain, respectively,  $f_t$ ,  $f_n$ , and m are a distributed tangential force, a distributed normal force, and a distributed moment along the rod axis, respectively,  $N_0$ ,  $T_0$ ,  $M_0$ ,  $N_L$ ,  $T_L$ , and  $M_L$  are a tangential force, a normal force, and a moment acting at s=0 and s=L, respectively.

# 3 | NURBS ELEMENTS

The basis functions of a NURBS curve are built from a knot vector. A knot vector  $\mathbf{\Xi} = \{\xi_1, \xi_2, \dots, \xi_{n+p+1}\}$  is a non-decreasing set of coordinates in the parametric space, where  $\xi_i$  is the ith knot, p is the polynomial degree, and n is the number of basis functions. Knot values may be repeated. The continuity of the basis functions at a knot is  $C^{p-m}$ , where m is the multiplicity of the knot. A knot vector is said to be open if its first and last knot values are repeated p+1 times. A knot span  $\Delta \xi_i$  is the difference between two consecutive knots, that is,  $\Delta \xi_i = \xi_{i+1} - \xi_i$ . Nonzero knot spans play the role of elements in FEA, that is, nonzero knot spans are the regions where numerical integration is performed.

Once the knot vector is defined, the B-spline basis functions are defined recursively starting with piecewise constants (p = 0)

$$M_{B,0}(\xi) = \begin{cases} 1 & \text{if } \xi_B \le \xi < \xi_{B+1}, \\ 0 & \text{otherwise.} \end{cases}$$
 (12)

For  $p = 1, 2, 3, \dots$ , the B-spline basis functions are defined by

$$M_{B,p}(\xi) = \frac{\xi - \xi_B}{\xi_{B+p} - \xi_B} M_{B,p-1}(\xi) + \frac{\xi_{B+p+1} - \xi}{\xi_{B+p+1} - \xi_{B+1}} M_{B+1,p-1}(\xi), \tag{13}$$

This is referred to as the Cox-de Boor recursion formula. <sup>2,61</sup> For evaluating this formula, whenever 0/0 is obtained, 0/0 is supposed to be substituted with 0. NURBS basis functions are defined as follows

$$N_B(\xi) = \frac{w_B M_{B,p}(\xi)}{\sum_{C=1}^n w_C M_{C,p}(\xi)},\tag{14}$$

where  $w_B$  is the Bth weight. The weights are needed to represent conic curves exactly. The reader is referred to Reference 2 for an explanation of how to use the knot insertion algorithm to perform h-refinement. In this work, we use open knot vectors and basis functions of degree p = 2.

The axis of the rod is obtained as a linear combination of the NURBS basis functions

$$\mathbf{r}(\xi) = \sum_{B=1}^{n} N_B(\xi) \mathbf{Q}_B, \tag{15}$$

where  $Q_B$  is the *B*th control point. Invoking the isoparametric concept, the tangential displacement, the normal displacement, and the rotation are discretized as follows

$$u^{h}(\xi) = \sum_{B=1}^{n} N_{B}(\xi) U_{B},$$

$$v^{h}(\xi) = \sum_{B=1}^{n} N_{B}(\xi) V_{B},$$

$$\theta^{h}(\xi) = \sum_{B=1}^{n} N_{B}(\xi) \Theta_{B},$$
(16)

where  $U_B$ ,  $V_B$ , and  $\Theta_B$  are the Bth control variable of the tangential displacement, the normal displacement, and the rotation, respectively. To discretize the virtual displacements, the Bubnov–Galerkin method is applied, that is,  $\delta u^h(\xi)$ ,  $\delta v^h(\xi)$ ,  $\delta \theta^h(\xi) \in \text{span}\{N_B(\xi)\}_{B=1}^n$ .

The use of the isoparametric concept and the Bubnov-Galerkin method yields the following element stiffness matrix

$$\mathbf{k} = \mathbf{k}_{\varepsilon} + \mathbf{k}_{\gamma} + \mathbf{k}_{\kappa},\tag{17}$$

$$\mathbf{k}_{\epsilon} = \begin{bmatrix} k_{\epsilon,bc}^{ij} \end{bmatrix}, \quad \mathbf{k}_{\gamma} = \begin{bmatrix} k_{\gamma,bc}^{ij} \end{bmatrix}, \quad \mathbf{k}_{\kappa} = \begin{bmatrix} k_{\kappa,bc}^{ij} \end{bmatrix}, \tag{18}$$

with

$$k_{\epsilon,bc}^{11} = \int_{s_{\epsilon}^{e}}^{s_{2}^{e}} \frac{dN_{b}}{ds} EA \frac{dN_{c}}{ds} ds, \quad k_{\epsilon,bc}^{12} = \int_{s_{\epsilon}^{e}}^{s_{2}^{e}} -\frac{dN_{b}}{ds} EA \frac{N_{c}}{R} ds, \quad k_{\epsilon,bc}^{22} = \int_{s_{\epsilon}^{e}}^{s_{2}^{e}} \frac{N_{b}}{R} EA \frac{N_{c}}{R} ds, \quad k_{\gamma,bc}^{11} = \int_{s_{\epsilon}^{e}}^{s_{2}^{e}} \frac{N_{b}}{R} \mu A \frac{N_{c}}{R} ds, \quad (19)$$

$$k_{\gamma,bc}^{12} = \int_{s_{\epsilon}^{e}}^{s_{\gamma}^{e}} \frac{N_{b}}{R} \mu A \frac{dN_{c}}{ds} ds, \quad k_{\gamma,bc}^{13} = \int_{s_{\epsilon}^{e}}^{s_{\gamma}^{e}} -\frac{N_{b}}{R} \mu A N_{c} ds, \quad k_{\gamma,bc}^{22} = \int_{s_{\epsilon}^{e}}^{s_{\gamma}^{e}} \frac{dN_{b}}{ds} \mu A \frac{dN_{c}}{ds} ds, \quad k_{\gamma,bc}^{23} = \int_{s_{\epsilon}^{e}}^{s_{\gamma}^{e}} -\frac{dN_{b}}{ds} \mu A N_{c} ds, \quad (20)$$

$$k_{\gamma,bc}^{33} = \int_{s^e}^{s_2^e} N_b \mu A N_c ds, \quad k_{\kappa,bc}^{33} = \int_{s^e}^{s_2^e} \frac{dN_b}{ds} E I \frac{dN_c}{ds} ds, \tag{21}$$

$$k_{e,bc}^{13} = k_{e,bc}^{23} = k_{e,bc}^{33} = k_{\kappa,bc}^{11} = k_{\kappa,bc}^{12} = k_{\kappa,bc}^{13} = k_{\kappa,bc}^{22} = k_{\kappa,bc}^{23} = 0,$$
 (22)

where  $s_1^e$  and  $s_2^e$  are the arc-length coordinates in which element e starts and ends, respectively,  $\mathbf{k}_{\varepsilon}$  is the element membrane stiffness matrix,  $\mathbf{k}_{\gamma}$  is the element shear stiffness matrix, and  $\mathbf{k}_{\kappa}$  is the element bending stiffness matrix. Only the upper triangular part of the element stiffness matrix is specified since the matrix is symmetric. Following standard FEA paraphernalia, the integrals above are computed performing change of variables twice. First, from the arc length coordinate s to the parametric coordinate s and then from the parametric coordinate s to the parent element with coordinate s to the parent element with coordinate s connectivity arrays. Since s is the element stiffness matrix is performed using conventional connectivity arrays.

# 4 | CAS ELEMENTS

The membrane and shear strains of a quadratic NURBS element have the following expressions

$$\epsilon^h(s) = \frac{du^h}{ds}(s) - \frac{v^h(s)}{R(s)},\tag{23}$$

$$\gamma^h(s) = \frac{u^h(s)}{R(s)} + \frac{dv^h}{ds}(s) - \theta^h(s),\tag{24}$$

respectively. CAS elements interpolate the membrane and shear strains at the knots using linear Lagrange polynomials resulting in a piecewise linear function for the membrane and shear strains. Thus, the membrane and shear strains of a CAS element are defined as follows

$$\epsilon^{\text{CAS},h}(s) = L_1(s)\epsilon^h(s_1^e) + L_2(s)\epsilon^h(s_2^e),\tag{25}$$

$$\gamma^{\text{CAS},h}(s) = L_1(s)\gamma^h(s_1^e) + L_2(s)\gamma^h(s_2^e), \tag{26}$$

with

$$L_1(s) = \frac{s_2^e - s}{s_2^e - s_1^e},\tag{27}$$

$$L_2(s) = \frac{s - s_1^e}{s_2^e - s_1^e},\tag{28}$$

where  $L_1$  and  $L_2$  are linear Lagrange polynomials and  $s_1^e$  and  $s_2^e$  are the arc-length coordinates which represent the start and the end of element e, respectively. If the multiplicity of a knot is one, that is, if the displacements and the rotation have  $C^1$  continuity at that knot, Equations (25) and (26) result in assumed strains that have  $C^0$  continuity across element boundaries. However, if the multiplicity of a knot is two, that is, if the displacements and the rotation have  $C^0$  continuity at that knot, Equations (25) and (26) result in assumed strains that are discontinuous at that knot. In both cases, the continuity of the assumed strains across element boundaries is the same as the continuity of the compatible strains across element boundaries. In practice, a repeated knot on a particular location is sometimes needed to represent a certain geometry exactly. When this locking treatment is applied to a knot vector in which the multiplicity of all interior knots is

two (i.e., when the locking treatment is applied to  $C^0$ -continuous quadratic NURBS), the resulting element type is named DAS elements. Comparisons among CAS and DAS elements are conducted in Section 5.

Equations (25) and (26) yield the following element stiffness matrix for CAS elements

$$\mathbf{k}^{\text{CAS}} = \mathbf{k}_{\epsilon}^{\text{CAS}} + \mathbf{k}_{\gamma}^{\text{CAS}} + \mathbf{k}_{\kappa},\tag{29}$$

$$\mathbf{k}_{\epsilon}^{\text{CAS}} = \left[ k_{\epsilon,bc}^{\text{CAS},ij} \right], \quad \mathbf{k}_{\gamma}^{\text{CAS}} = \left[ k_{\gamma,bc}^{\text{CAS},ij} \right], \quad \mathbf{k}_{\kappa} = \left[ k_{\kappa,bc}^{ij} \right],$$
 (30)

with

$$k_{\epsilon,bc}^{\text{CAS},11} = \sum_{l=1}^{2} \sum_{m=1}^{2} \int_{s^{\epsilon}}^{s^{\epsilon}_{2}} L_{l}(s) \frac{dN_{b}}{ds}(s_{l}^{e}) EAL_{m}(s) \frac{dN_{c}}{ds}(s_{m}^{e}) ds, \quad k_{\epsilon,bc}^{\text{CAS},12} = \sum_{l=1}^{2} \sum_{m=1}^{2} \int_{s^{\epsilon}}^{s^{\epsilon}_{2}} -L_{l}(s) \frac{dN_{b}}{ds}(s_{l}^{e}) EAL_{m}(s) \frac{N_{c}(s_{m}^{e})}{R(s_{m}^{e})} ds, \quad (31)$$

$$k_{\epsilon,bc}^{\text{CAS},22} = \sum_{l=1}^{2} \sum_{m=1}^{2} \int_{s_{\epsilon}^{e}}^{s_{\epsilon}^{e}} L_{l}(s) \frac{N_{b}(s_{l}^{e})}{R(s_{l}^{e})} EAL_{m}(s) \frac{N_{c}(s_{m}^{e})}{R(s_{m}^{e})} ds, \quad k_{\gamma,bc}^{\text{CAS},11} = \sum_{l=1}^{2} \sum_{m=1}^{2} \int_{s_{\epsilon}^{e}}^{s_{\epsilon}^{e}} L_{l}(s) \frac{N_{b}(s_{l}^{e})}{R(s_{l}^{e})} \mu AL_{m}(s) \frac{N_{c}(s_{m}^{e})}{R(s_{m}^{e})} ds, \quad (32)$$

$$k_{\gamma,bc}^{\text{CAS},12} = \sum_{l=1}^{2} \sum_{m=1}^{2} \int_{s_{l}^{e}}^{s_{l}^{e}} L_{l}(s) \frac{N_{b}(s_{l}^{e})}{R(s_{l}^{e})} \mu A L_{m}(s) \frac{dN_{c}}{ds}(s_{m}^{e}) ds, \quad k_{\gamma,bc}^{\text{CAS},13} = \sum_{l=1}^{2} \sum_{m=1}^{s_{l}^{e}} \int_{s_{l}^{e}}^{s_{l}^{e}} -L_{l}(s) \frac{N_{b}(s_{l}^{e})}{R(s_{l}^{e})} \mu A L_{m}(s) N_{c}(s_{m}^{e}) ds, \quad (33)$$

$$k_{\gamma,bc}^{\text{CAS},22} = \sum_{l=1}^{2} \sum_{m=1}^{2} \int_{s^e}^{s^e_{l}} L_l(s) \frac{dN_b}{ds}(s^e_l) \mu A L_m(s) \frac{dN_c}{ds}(s^e_m) ds, \quad k_{\gamma,bc}^{\text{CAS},23} = \sum_{l=1}^{2} \sum_{m=1}^{2} \int_{s^e}^{s^e_{l}} -L_l(s) \frac{dN_b}{ds}(s^e_l) \mu A L_m(s) N_c(s^e_m) ds, \quad (34)$$

$$k_{\gamma,bc}^{\text{CAS},33} = \sum_{l=1}^{2} \sum_{m=1}^{2} \int_{s^{e}}^{s^{e}_{2}} L_{l}(s) N_{b}(s^{e}_{l}) \mu A L_{m}(s) N_{c}(s^{e}_{m}) ds, \quad k_{\kappa,bc}^{33} = \int_{s^{e}}^{s^{e}_{2}} \frac{dN_{b}}{ds} EI \frac{dN_{c}}{ds} ds,$$
 (35)

$$k_{\epsilon,bc}^{\text{CAS},13} = k_{\epsilon,bc}^{\text{CAS},23} = k_{\epsilon,bc}^{\text{CAS},33} = k_{\kappa,bc}^{11} = k_{\kappa,bc}^{12} = k_{\kappa,bc}^{13} = k_{\kappa,bc}^{22} = k_{\kappa,bc}^{23} = 0,$$
(36)

where  $\mathbf{k}^{\text{CAS}}$  is the element stiffness matrix of CAS elements,  $\mathbf{k}^{\text{CAS}}_{\epsilon}$  is the element membrane stiffness matrix of CAS elements, and  $\mathbf{k}^{\text{CAS}}_{\gamma}$  is the element shear stiffness matrix of CAS elements. Only the upper triangular part of the element stiffness matrix is specified since the matrix is symmetric. As in Section 3, the integrals above are computed performing change of variables twice  $(s \to \xi \to \hat{\xi})$ . In the parent element,  $L_r(\hat{\xi}) = (1 + (-1)^r \hat{\xi})/2$ . The assembly of the element stiffness matrices into the global stiffness matrix is performed using conventional connectivity arrays.<sup>2,62</sup>

When stress resultants are computed using CAS elements, the membrane and shear forces are obtained as

$$\mathcal{N}^{\text{CAS},h} = EA\epsilon^{\text{CAS},h},\tag{37}$$

$$\mathcal{T}^{CAS,h} = \mu A \gamma^{CAS,h}, \tag{38}$$

respectively.

Remark 1. In Reference 50, the authors of this article proposed the element type CAS elements to remove membrane locking from NURBS-based discretizations of Kirchhoff rods. In this section, the element type CAS elements was extended to remove shear and membrane locking from NURBS-based discretizations of Timoshenko rods. The element type DAS elements defined in this section cannot be applied to Kirchhoff rods since Kirchhoff rods is a fourth-order theory whose discretization using the Galerkin method requires basis functions with  $C^1$  continuity across element boundaries.

#### 5 NUMERICAL EXPERIMENTS

In this section, we perform numerical investigations using the discretizations described in Sections 3 and 4. The code used to perform these simulations has been developed on top of the PetIGA framework, 63 which adds NURBS discretization capabilities and integration of forms to the scientific library PETSc.  $^{64}$  A Gauss-Legendre quadrature rule with p+1 integration points is used to compute all the integrals unless specifically mentioned otherwise. In this section,  $n_{cp}$  denotes the number of control points and  $n_{el}$  denotes the number of elements.

We use exact solutions to study the convergence in  $L^2$  norm of the tangential displacement, the normal displacement, the rotation, the membrane force, the shear force, and the bending moment. In order to do so, we define the relative errors in  $L^2$  norm of the tangential displacement, the normal displacement, the rotation, the membrane force, the shear force, and the bending moment as

$$e_{L^{2}}(u^{h}) = \frac{\sqrt{\int_{0}^{L} (u^{h} - u)^{2} ds}}{\sqrt{\int_{0}^{L} u^{2} ds}}, \quad e_{L^{2}}(v^{h}) = \frac{\sqrt{\int_{0}^{L} (v^{h} - v)^{2} ds}}{\sqrt{\int_{0}^{L} v^{2} ds}}, \quad e_{L^{2}}(\theta^{h}) = \frac{\sqrt{\int_{0}^{L} (\theta^{h} - \theta)^{2} ds}}{\sqrt{\int_{0}^{L} \theta^{2} ds}}, \\ e_{L^{2}}(\mathcal{N}^{h}) = \frac{\sqrt{\int_{0}^{L} (\mathcal{N}^{h} - \mathcal{N})^{2} ds}}{\sqrt{\int_{0}^{L} \mathcal{N}^{2} ds}}, \quad e_{L^{2}}(\mathcal{T}^{h}) = \frac{\sqrt{\int_{0}^{L} (\mathcal{T}^{h} - \mathcal{T})^{2} ds}}{\sqrt{\int_{0}^{L} \mathcal{N}^{2} ds}}, \quad e_{L^{2}}(\mathcal{M}^{h}) = \frac{\sqrt{\int_{0}^{L} (\mathcal{M}^{h} - \mathcal{M})^{2} ds}}{\sqrt{\int_{0}^{L} \mathcal{N}^{2} ds}},$$

$$(39)$$

respectively. Since we are solving second-order differential equations with basis functions of degree 2, the optimal convergence rates of  $e_{L^2}(u^h)$ ,  $e_{L^2}(v^h)$ ,  $e_{L^2}(\mathcal{N}^h)$ ,  $e_{L^2}(\mathcal{N}^h)$ ,  $e_{L^2}(\mathcal{T}^h)$ , and  $e_{L^2}(\mathcal{M}^h)$  are 3, 3, 3, 2, 2, and 2, respectively.<sup>62</sup> In engineering applications, discretization errors are acceptable in case they are smaller than the model errors (errors between reality and the mathematical model). Since errors in Equation (39) are relative errors, values of the errors equal to  $10^{-2}$  (1% errors) are accurate enough for most engineering applications.

# 5.1 | Clamped quarter-circular arc with a moment applied at the free end

We start our numerical investigation with a pure bending problem. This problem consists of a quarter-circle rod clamped at one end and free at the other end. A moment is acting on the free end. The geometry of the rod, the boundary conditions, and the load are shown in Figure 2. The cross-section of the rod is a rectangle with dimensions d and t. Thus, A = td and  $I = dt^3/12$ . The remaining parameters that play a role in this problem have the following values

$$R = 1.0, \quad M_L = 10^6 t^3, \quad E = 1.0 \times 10^9, \quad \mu = 5.0 \times 10^8, \quad d = 0.2.$$
 (40)

We solve this problem for R/t = 10,  $R/t = 10^2$ , and  $R/t = 10^3$  by selecting the value of the thickness as t = 0.1, t = 0.01, and t = 0.001, respectively. In Reference 65, the exact value of the normal displacement at the free end of the rod (denoted by point B in Figure 2) is given as

$$v_B = \frac{M_L R^2}{EI}. (41)$$

We initiate our convergence study with a uniform mesh composed of two  $C^1$ -continuous quadratic elements. Subsequently, we carry out uniform h-refinement seven times using the knot insertion algorithm. The axis of the rod is

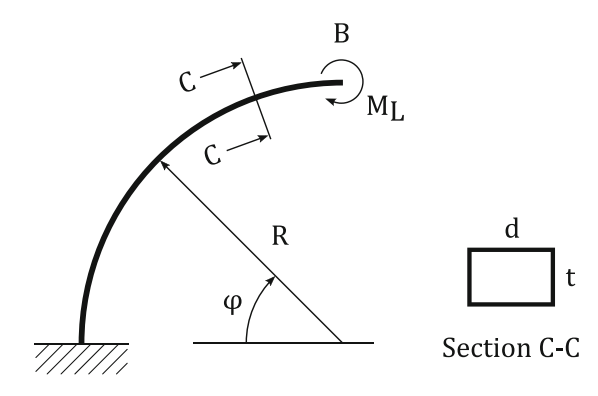


FIGURE 2 Geometry, boundary conditions, and applied load for the clamped quarter-circular arch with a moment at the free end.

represented exactly since we are using quadratic NURBS. Figure 3 plots the convergence of the normal displacement at point B using CAS and NURBS elements. As shown in Figure 3, the convergence of NURBS elements heavily worsens as the slenderness ratio increases. In contrast, the convergence of CAS elements is independent of the slenderness ratio for the broad range of R/t values considered in this example.

Figure 4 plots the distributions of the membrane and shear forces for R/t = 10 using 8, 32, and 128 NURBS elements. Since this is a pure bending problem, the exact solution of the membrane and shear forces is zero. However, when using NURBS elements, even for a thick rod (R/t = 10), membrane and shear locking result in large-amplitude oscillations of the membrane and shear forces for coarse and fine meshes as shown in Figure 4. In contrast, the values of the membrane and shear forces are negligible using CAS elements, namely, the absolute value of the membrane and shear forces is smaller than  $10^{-6}$  for R/t = 10,  $10^{2}$ , and  $10^{3}$  and mesh resolutions ranging from 2 elements to 256 elements. Thus, CAS elements are an effective numerical scheme to remove shear and membrane locking.

# 5.2 | Clamped-clamped semi-circular arc under a distributed load

The second numerical investigation deals with a clamped-clamped semi-circular arch under a distributed load as shown in Figure 5A. Since the problem is symmetric, we solve for half of the arch with the appropriate symmetry boundary conditions shown in Figure 5B. The next values are used in this example

$$q = 10^6 t^3$$
,  $R = 10.0$ ,  $E = 2.1 \times 10^{11}$ ,  $v = 0.28$ ,  $d = 0.1$ , (42)

Slenderness ratios of  $R/t = 10^2$ ,  $R/t = 10^3$ , and  $R/t = 10^4$  are studied by selecting t = 0.1, t = 0.01, and t = 0.001, respectively. The cross section of the rod is a rectangle. Thus, A = td and  $I = t^3d/12$ . q is a distributed load per unit of horizontal length while  $f_t$  and  $f_n$  in Equation (11) are distributed loads per unit length along the axis of the rod. Hence,  $f_t = -q \sin(\varphi) \cos(\varphi)$  and  $f_n = q \sin(\varphi) \sin(\varphi)$ , where the angle  $\varphi$  is shown in Figure 5B.

The exact solution to this problem is written in Reference 65, namely,

$$u = A_1 \left[ c_1 \varphi \sin(\varphi) - c_3 R \left( 1 - \cos(\varphi) \right) \right] - A_2 c_3 \left( \varphi - \sin(\varphi) \right) + A_3 \sin(\varphi)$$

$$- q R \left[ \sin(2\varphi) \left( (2/3)c_1 - (1/6)c_2 - 0.125c_3 R \right) - 0.5 \varphi c_3 R \right],$$
(43)

$$v = A_1 \left[ c_1 \left( \varphi \cos(\varphi) - \sin(\varphi) \right) + c_2 \sin(\varphi) - c_3 R \sin(\varphi) \right] - A_2 c_3 \left( 1 - \cos(\varphi) \right) + A_3 \cos(\varphi)$$

$$+ q R \left[ c_1 - 0.5 c_2 + 0.5 c_3 R - \cos(2\varphi) \left( (1/3) c_1 + (1/6) c_2 - 0.25 c_3 R \right) \right], \tag{44}$$

$$\theta = -A_2(\varphi/R)c_3 + A_1c_3(\cos(\varphi) - 1) + qRc_3(0.5\varphi + 0.125\sin(2\varphi)), \tag{45}$$

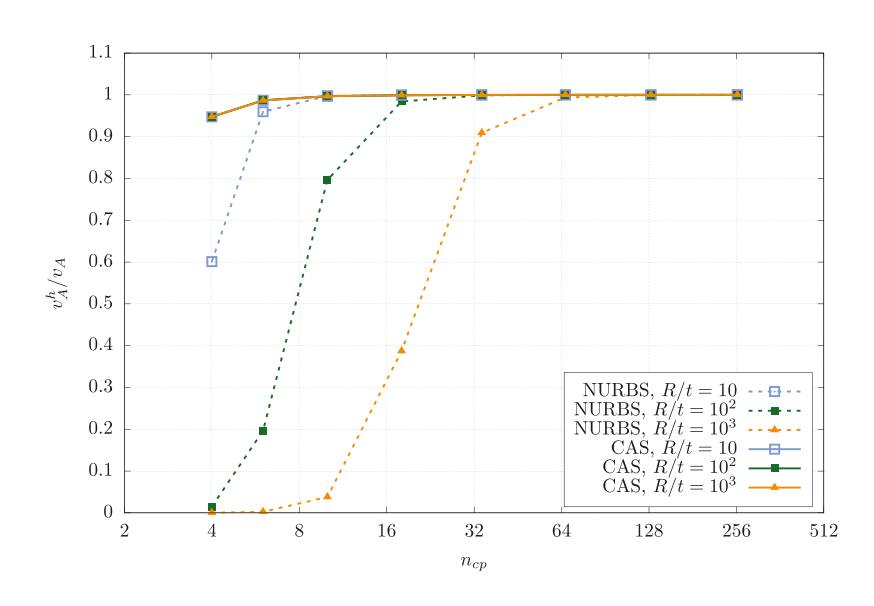


**FIGURE 3** (Color online) Clamped quarter-circular arc with a moment applied at the free end. Convergence of the deflection at point B using NURBS elements and CAS elements. For the ample range considered, the convergence of CAS elements is independent of the slenderness ratio.

10970207, 0, Downloaded from https://onlinelibrary.wiley.com/doi/10.1002/nme.7257, Wiley Online Library on [28/07/2023]. See the Terms and Conditions (https://onlinelibrary.wiley.com/terms-and-conditions) on Wiley Online Library for rules of use; OA articles are governed by the applicable Creative Commons License

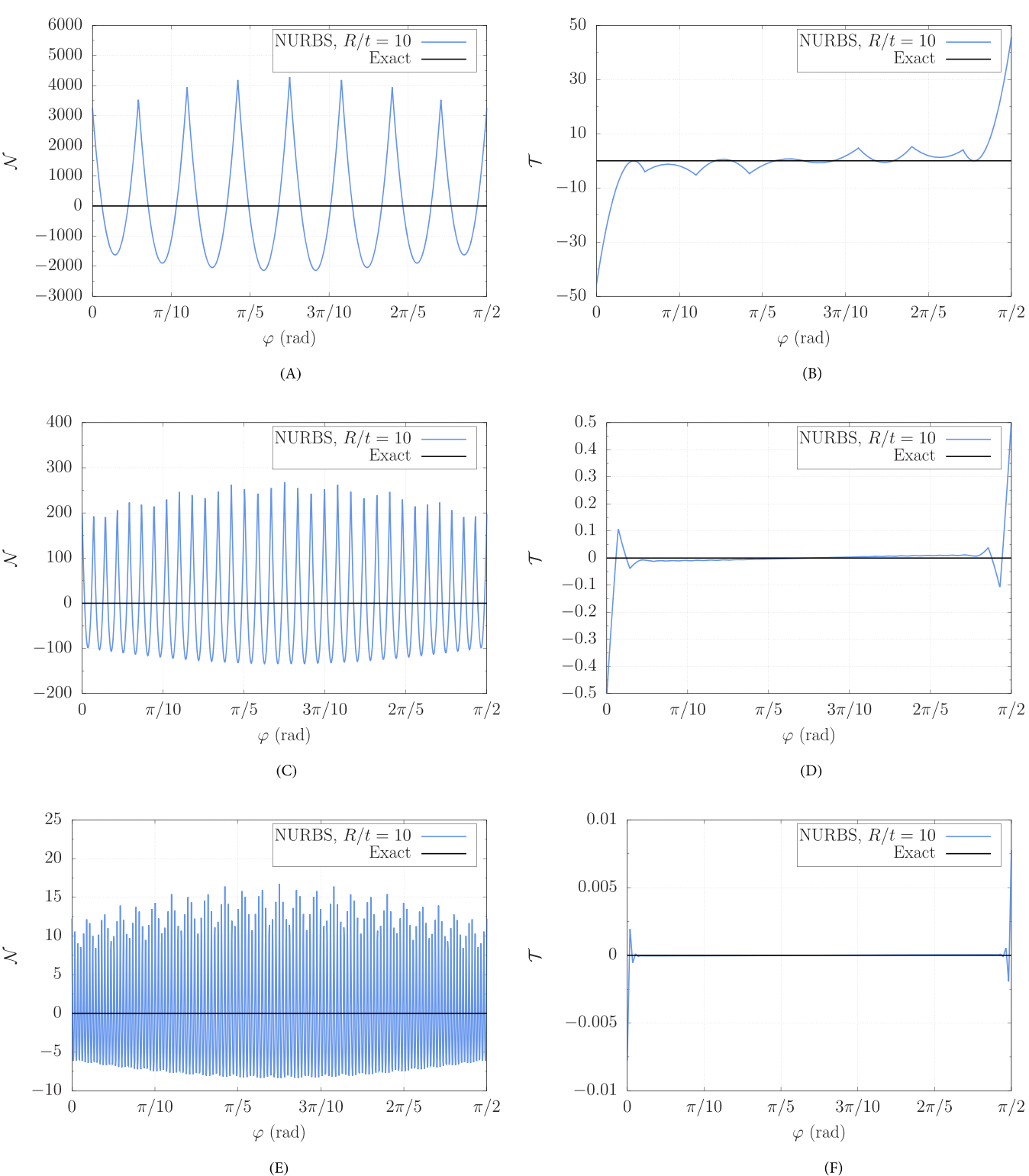


**FIGURE 4** (Color online) Clamped quarter-circular arch with a moment applied at the free end. Membrane and shear forces for R/t = 10 using (A, B) 8, (C, D) 32, and (E, F) 128 NURBS elements. For this problem, the exact solution of the membrane and shear forces is zero. The numerical solutions using NURBS elements lock resulting in large-amplitude spurious oscillations. However, the values of the membrane and shear forces using CAS elements are negligible, namely, the absolute value of the membrane and shear forces are smaller than  $10^{-6}$  for all the slenderness ratios and mesh resolutions considered in this example.

**FIGURE 5** Geometry, boundary conditions, and applied load for the clamped-clamped semi-circular arch under a distributed load. (A) Before applying symmetry. (B) After applying symmetry.

$$\mathcal{N} = A_1 \sin(\varphi) - qR\cos^2(\varphi), \tag{46}$$

$$\mathcal{T} = A_1 \cos(\varphi) + qR \cos(\varphi) \sin(\varphi), \tag{47}$$

$$\mathcal{M} = -A_1 R \sin(\varphi) - A_2 + 0.5 q R^2 (1 + 0.5 \cos(2\varphi)), \tag{48}$$

with

$$c_1 = \frac{1}{2} \left( \frac{R}{EA} + \frac{R}{\mu A} + \frac{R^3}{EI} \right), \quad c_2 = \left( \frac{R}{\mu A} + \frac{R^3}{EI} \right), \quad c_3 = \frac{R^2}{EI}.$$
 (49)

$$A_1 = \frac{8\pi q (c_1 - c_2) + 3\pi q R c_3}{6\pi^2 (c_1/R) - 24c_3},$$
(50)

$$A_2 = \frac{qR^2}{2} - \frac{16\pi qR (c_1 - c_2) + 6\pi qR^2 c_3}{6\pi^3 (c_1/R) - 24\pi c_3},$$
(51)

$$A_3 = -\frac{2qR(c_1 - c_2)}{3} - \frac{3qR^2c_3}{4}. (52)$$

In order to study the convergence of NURBS and CAS elements, we construct a uniform mesh consisting of two  $C^1$ -continuous quadratic elements. Then, we refine this mesh by applying uniform h-refinement seven times. Figure 6 shows the convergence in  $L^2$  norm of the tangential and normal displacements, the rotation, the membrane force, the shear force, and the bending moment using NURBS and CAS elements. As shown in Figure 6, the convergence curves of NURBS elements heavily deteriorate as the slenderness ratio increases. In addition, Figure 6D,E reveals an anomalous behavior in the convergence of the membrane and shear forces using NURBS elements, namely, the relative error in  $L^2$  norm of the membrane and shear forces increases as uniform h-refinement is performed multiple times (the relative error of the membrane and shear forces is greater than 100% for most mesh resolutions and slenderness ratios). This type of anomalous behavior was reported for the membrane force in discretizations of Kirchhoff rods based on B-splines<sup>4</sup> and NURBS.<sup>50</sup> However, to the authors knowledge, it has not been reported for Timoshenko rods before. In contrast, the convergence curves of CAS elements for  $R/t = 10^2$ ,  $R/t = 10^3$ , and  $R/t = 10^4$  overlap (with the exception of the fine meshes for  $R/t = 10^4$  which undergo slight differences). The convergence rates of  $e_{L^2}(u^h)$ ,  $e_{L^2}(v^h)$ ,  $e_{L^2}(\rho^h)$ ,  $e_{L^2}(\mathcal{N}^h)$ ,  $e_{L^2}(\mathcal{N}^h)$ ,  $e_{L^2}(\mathcal{N}^h)$ , and  $e_{L^2}(\mathcal{M}^h)$  using CAS elements are 2, 2, 2, 1.5, 1.5, and 1.5, respectively. Note that the relative error in  $L^2$  norm of the membrane and shear forces obtained with CAS elements is multiple orders of magnitude smaller than that of NURBS elements. As in Section 5.1, CAS elements remove shear and membrane locking for an ample range of slenderness ratios.

 $10^{+1}$ 

 $10^{0}$ 

 $10^{-1}$ 

 $10^{-2}$ 

 $10^{-3}$ 

 $10^{-4}$ 

 $10^{-5}$ 

 $10^{-6}$ 

 $10^{-7}$ 

 $10^{-8}$ 2

 $10^{+1}$ 

 $10^{0}$ 

 $10^{-1}$ 

 $10^{-2}$ 

 $10^{-3}$ 

 $10^{-4}$ 

 $10^{-5}$ 

 $10^{-6}$ 

 $10^{-7}$ 

 $10^{-8}$ 2

 $10^{+4}$ 

 $10^{+3}$  $\tilde{10^{+2}}$ 

 $10^{+1}$  $10^{0}$ 

 $10^{-1}$  $10^{-2}$ 

 $10^{-3}$ 

 $10^{-4}$ 

 $10^{-5}$ 

 $10^{-6}$  $10^{-7}$ 

 $10^{-8}$ 

 $10^{-9}$ 

 $10^{-10}$ 

 $10^{-11}$ 

 $10^{-12}$ 

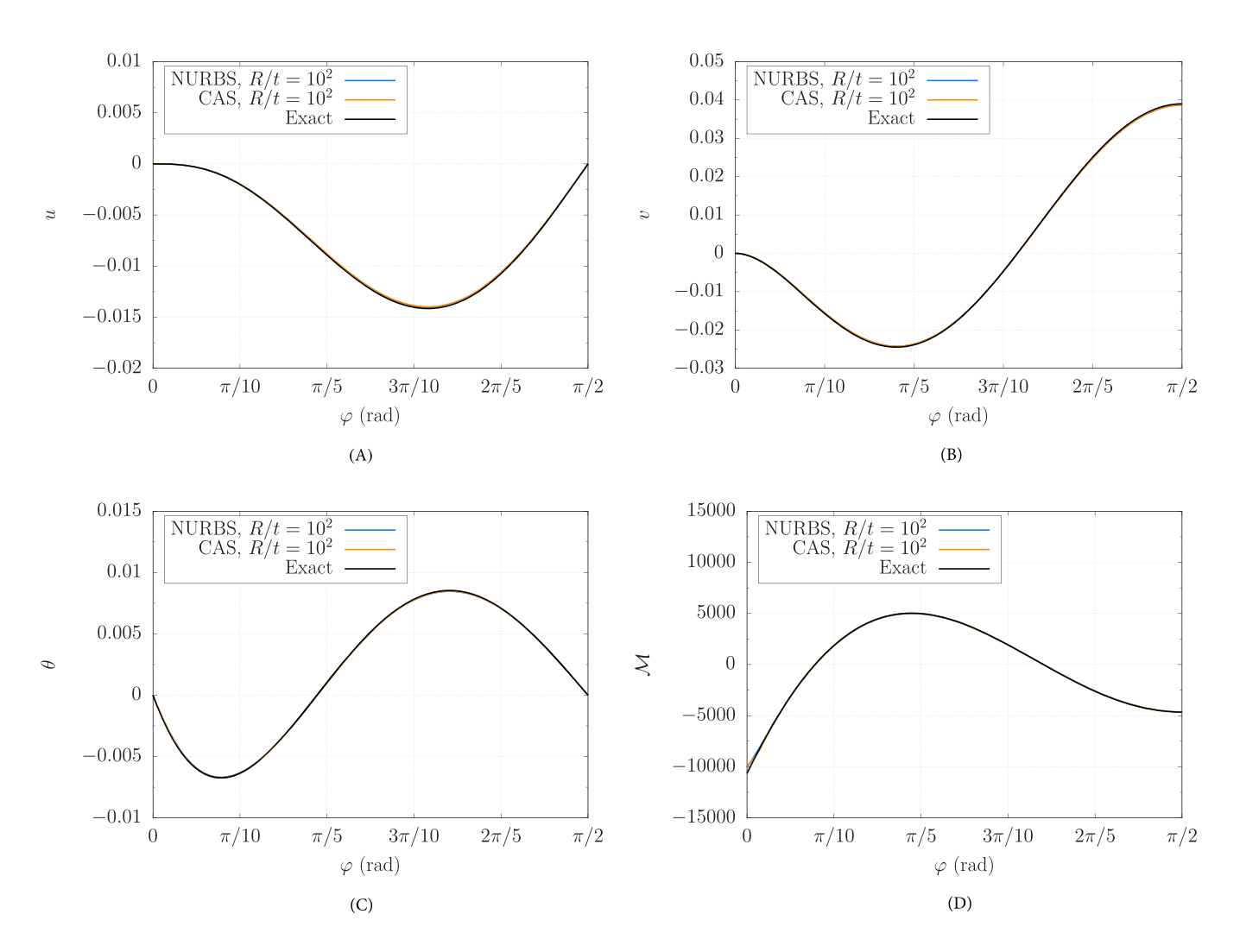
2

4

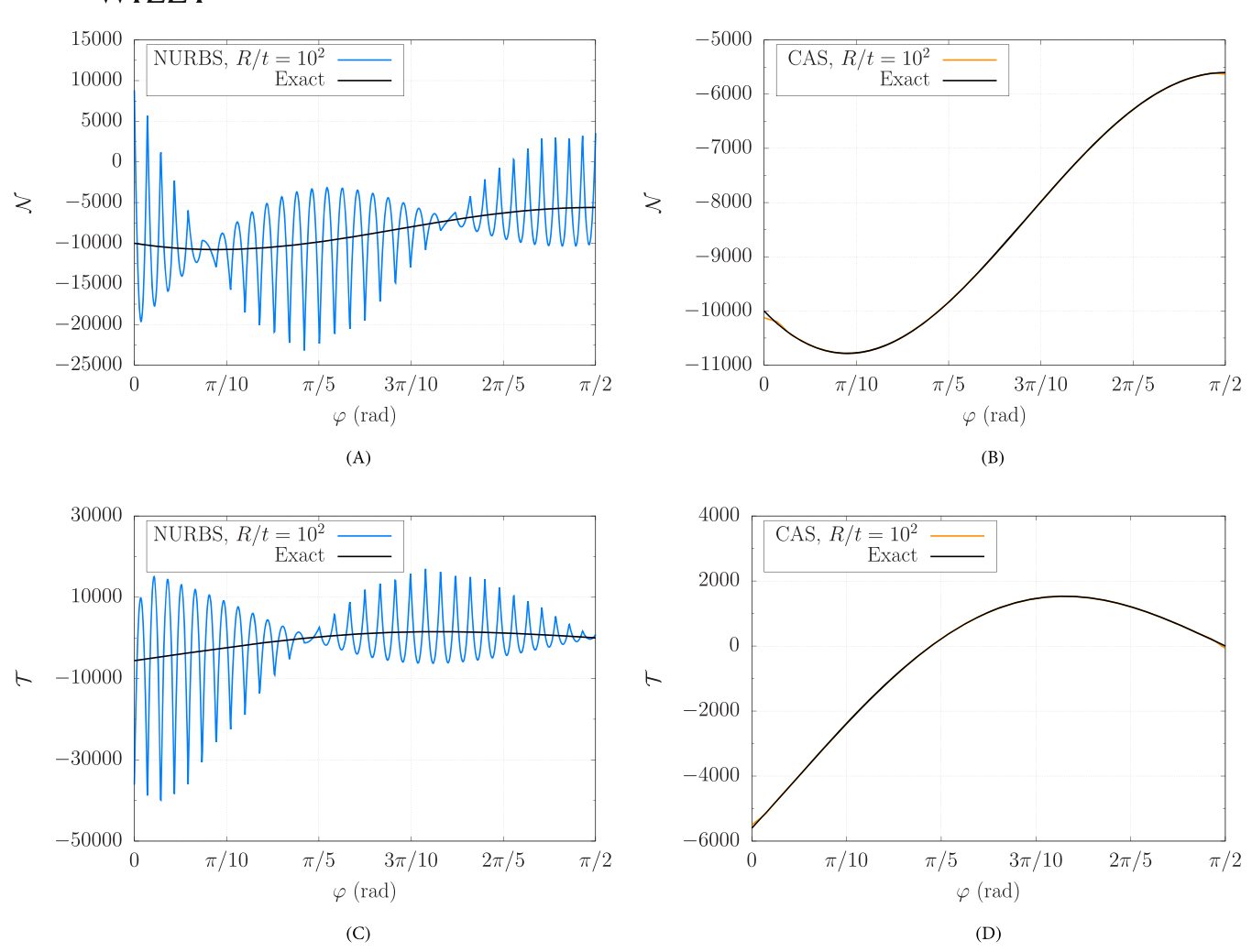
8

FIGURE 6 (Color online) Clamped-clamped semi-circular arc under a distributed load. Convergence of the (A) tangential and (B) normal displacements, (C) the rotation, (D) the membrane force, (E) the shear force, and (F) the bending moment using NURBS elements and CAS elements. For any of the slenderness ratios considered, CAS elements overcomes locking.

The results plotted in Figure 6 show that it is not enough to only evaluate the accuracy of displacements and rotations to decide whether or not a certain numerical scheme is effective in overcoming shear and membrane locking. The reason is that  $e_{L^2}(\mathcal{N}^h)$  and  $e_{L^2}(\mathcal{T}^h)$  can have unreasonably high values while  $e_{L^2}(u^h)$ ,  $e_{L^2}(v^h)$ ,  $e_{L^2}(\theta^h)$ , and  $e_{L^2}(\mathcal{M}^h)$  have low values. In order to better show this, Figures 7 and 8 plot the distributions of the tangential and normal displacements, the rotation, the membrane force, the shear force, and the bending moment for  $R/t = 10^2$  using 32 elements. As shown in Figures 7 and 8, when using NURBS elements, the distributions of tangential and normal displacements, the rotation, and the bending moment are accurate while shear and membrane locking cause large-amplitude spurious oscillations in the distributions of the shear and membrane forces. The absolute value of the maximum shear force obtained with NURBS elements divided by the maximum exact shear force is 7.12 while the absolute value of the maximum membrane force obtained with NURBS elements divided by the maximum exact membrane force is 2.15. On the contrary, all the distributions are accurate when using CAS elements. Figures 9 and 10 plot the distributions of the tangential and normal displacements, the rotation, the membrane force, the shear force, and the bending moment using 32 elements, but for  $R/t = 10^4$ . As shown in Figures 9 and 10, when using NURBS elements, shear and membrane locking cause the distributions of tangential and normal displacements, the rotation, and the bending moment to have zero values and the shear and membrane forces to have large-amplitude spurious oscillations. The absolute value of the maximum shear force obtained with NURBS elements divided by the maximum exact shear force is 547.38 while the absolute value of the maximum membrane force obtained with NURBS elements divided by the maximum exact membrane force is 152.96. As for  $R/t = 10^2$ , all the distributions are accurate when using CAS elements.



**FIGURE** 7 (Color online) Clamped-clamped semi-circular arc under a distributed load. Distributions of the (A) tangential and (B) normal displacements, (C) the rotation, and (D) the bending moment using NURBS elements and CAS elements. The mesh has 32 elements and  $R/t = 10^2$ . Both NURBS elements and CAS elements result in accurate distributions.



**FIGURE** 8 (Color online) Clamped-clamped semi-circular arc under a distributed load. Distributions of the membrane and shear forces using (A, C) NURBS and (B, D) CAS elements. The mesh has 32 elements and  $R/t = 10^2$ . The numerical solution using NURBS elements has large-amplitude spurious oscillations while such spurious oscillations disappear when using CAS elements. Note the different vertical scale used in each plot.

Next, we compare the convergence of CAS elements and DAS elements. The locking treatment of CAS and DAS elements is the same. CAS elements applies the locking treatment to  $C^1$ -continuous quadratic NURBS while DAS elements applies the locking treatment to  $C^0$ -continuous quadratic NURBS. Whenever the accuracy of  $C^{p-1}$ -continuous NURBS basis functions is compared with the accuracy of  $C^0$ -continuous NURBS basis functions, the comparison should be done with respect to both the number of control points  $(n_{cv})$  and the number of elements  $(n_{el})^*$ . The reason is that the comparison with respect to the number of control points is advantageous for  $C^{p-1}$ -continuous NURBS basis functions (for a given number of control points,  $C^{p-1}$ -continuous NURBS basis functions have significantly more elements than  $C^0$ -continuous NURBS basis functions) while the comparison with respect to the number of elements is advantageous to  $C^0$ -continuous NURBS basis functions (for a given number of elements, C<sup>0</sup>-continuous NURBS basis functions have significantly more control points than  $C^{p-1}$ -continuous NURBS basis functions). Figure 11 shows the convergence in  $L^2$  norm of the tangential and normal displacements, the rotation, the membrane force, the shear force, and the bending moment with respect to the number of control points while Figure 12 shows the convergence in  $L^2$  norm of the tangential and normal displacements, the rotation, the membrane force, the shear force, and the bending moment with respect to the number of elements. As shown in Figures 11 and 12, the convergence curves of DAS elements for  $R/t = 10^2$ ,  $R/t = 10^3$ , and  $R/t = 10^4$  overlap. Thus, DAS elements also effectively remove shear and membrane locking for the ample range of slenderness ratios considered. However, it is clear from Figures 11 and 12 that the accuracy of CAS elements is higher than the accuracy of DAS elements.



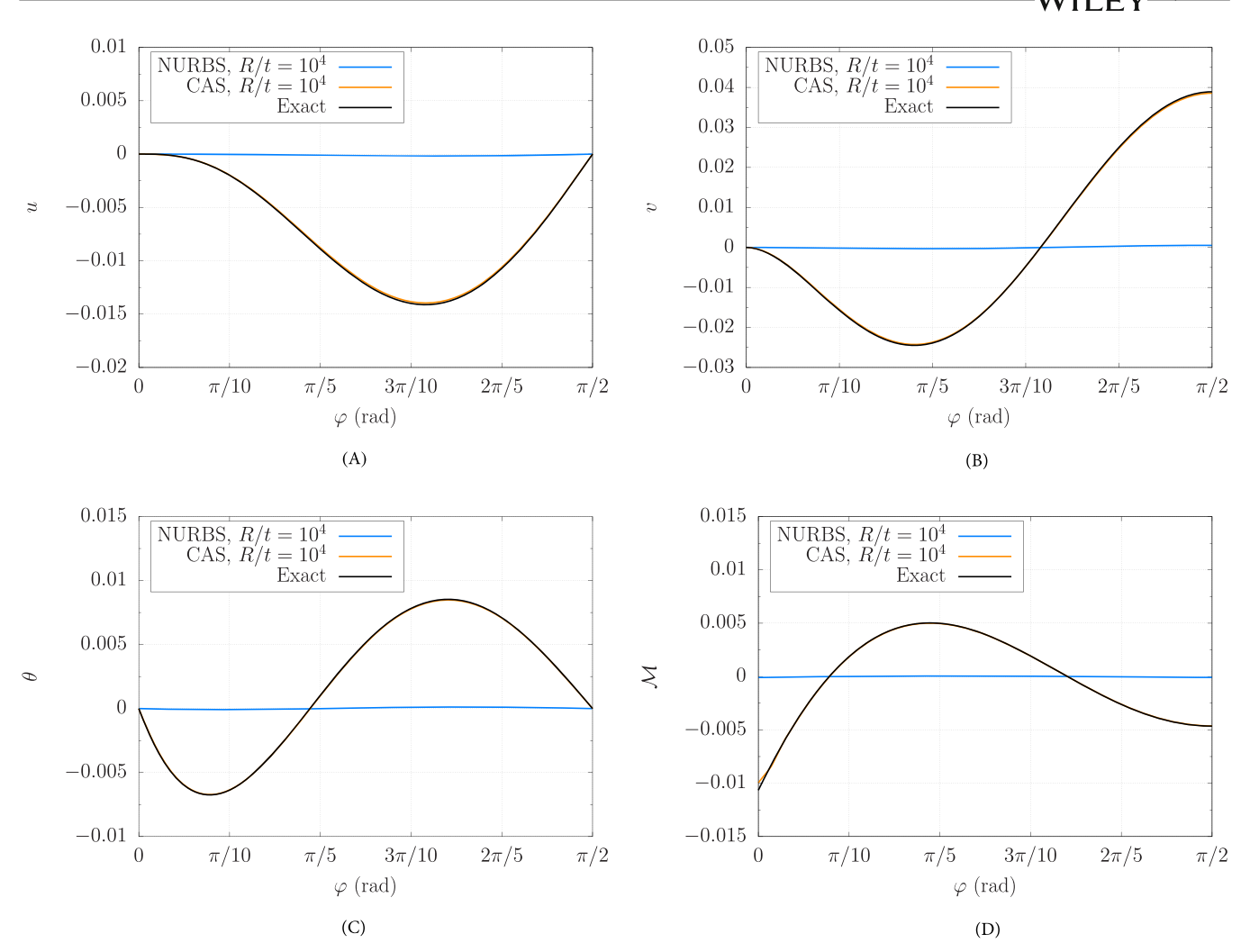


**FIGURE 9** (Color online) Clamped-clamped semi-circular arc under a distributed load. Distributions of the (A) tangential and (B) normal displacements, (C) the rotation, and (D) the bending moment using NURBS elements and CAS elements. The numerical solution using NURBS elements has zero values while the numerical solution using CAS elements and the exact solution overlap at the scale of the plot. The mesh has 32 elements and  $R/t = 10^4$ .

Discretizations of rod theories based on the Galerkin method and the isoparametric concept are known to result in stiffness matrices with quite high condition numbers. For  $R/t = 10^3$ , Table 1 specifies the condition number obtained with NURBS elements, CAS elements, DAS elements, and standard finite elements (linear Lagrange polynomials with 2 Gauss–Legendre quadrature points). As shown in Table 1, quadratic NURBS do not increase the condition number with respect to linear Lagrange polynomials, but mildly decrease it. In addition, the high values of the condition number is not what causes shear and membrane locking since CAS elements and NURBS elements have similar condition numbers, but CAS elements are locking-free for  $R/t = 10^3$  while NURBS elements lock.

# 5.3 | Simply-supported straight rod under a distributed load

The last numerical investigation addresses a simply-supported straight rod under a distributed load. The geometry, the boundary conditions, and the load are shown in Figure 13. Since the cross section of the rod is a rectangle, A = td and  $I = t^3d/12$ . The next values are used in this example

$$q = 10^5 t^3$$
,  $L = 20.0$ ,  $E = 2.1 \times 10^{11}$ ,  $v = 0.28$ ,  $d = 1$ . (53)

For this problem, the slenderness ratio is defined as L/t. We solve this problem for three slenderness ratios, namely,  $L/t = 10^2$ ,  $L/t = 10^3$ , and  $L/t = 10^4$ , which are obtained by selecting t = 0.2, t = 0.02, and t = 0.002, respectively. This

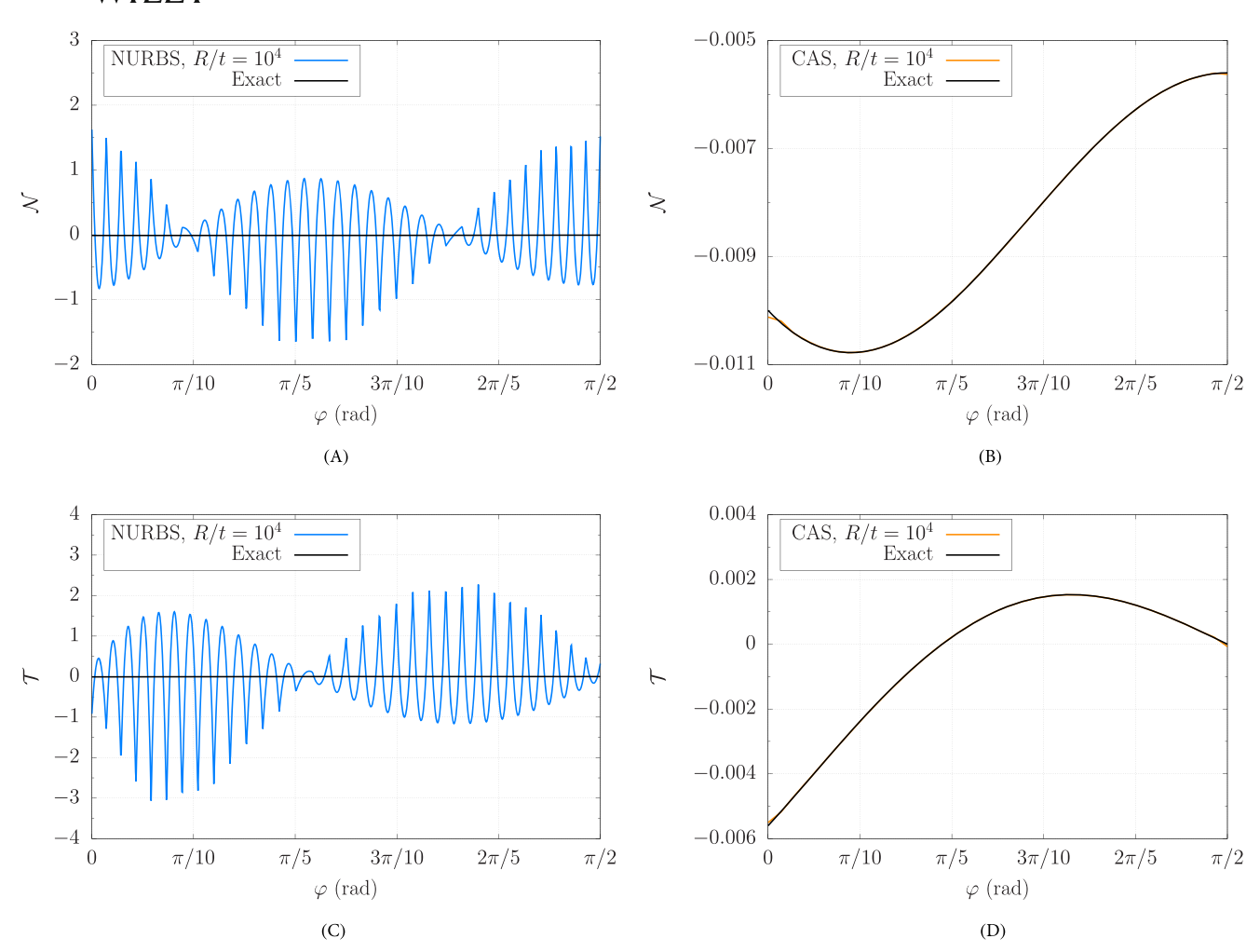


**FIGURE 10** (Color online) Clamped-clamped semi-circular arc under a distributed load. Distributions of the membrane and shear forces using (A, C) NURBS and (B, D) CAS elements. The mesh has 32 elements and  $R/t = 10^4$ . The numerical solution using NURBS elements has large-amplitude spurious oscillations while such spurious oscillations disappear when using CAS elements. Note the different vertical scale used in each plot.

problem has the following exact solution

$$v(s) = \frac{qL^4}{24EI} \left( \frac{s}{L} - 2\frac{s^3}{L^3} + \frac{s^4}{L^4} \right) + \frac{qL^2}{24\mu A} \left( \frac{s}{L} - \frac{s^2}{L^2} \right), \tag{54}$$

$$\theta(s) = \frac{qL^3}{24EI} \left( 1 - 6\frac{s^2}{L^2} + 4\frac{s^3}{L^3} \right),\tag{55}$$

$$\mathcal{M}(s) = -\frac{qL^2}{2} \left( \frac{s}{L} - \frac{s^2}{L^2} \right),\tag{56}$$

$$\mathcal{T}(s) = \frac{qL}{2} \left( 1 - 2\frac{s}{L} \right). \tag{57}$$

As in the preceding sections, we start our convergence study with a uniform mesh composed of two  $C^1$ -continuous quadratic elements and then perform uniform h-refinement seven times. Figure 14 plots the convergence in  $L^2$  norm of the normal displacement, the rotation, the shear force, and the bending moment using NURBS and CAS elements. As shown in Figure 14, the convergence of NURBS elements heavily deteriorates as L/t increases due to shear locking. In contrast, CAS elements overcome shear locking satisfactorily. Note that the convergence patterns of  $e_{L^2}(\mathcal{T}^h)$  using CAS elements are specific to this particular problem since the exact solution of the shear force is a linear polynomial (see Equation 57).

10970207, 0, Downloaded from https://onlinelibrary.wiley.com/doi/10.1002/nme.257, Wiley Online Library on [28/07/2023]. See the Terms and Conditions (https://onlinelibrary.wiley.com/terms-and-conditions) on Wiley Online Library for rules of use; OA articles are governed by the applicable Creative Commons Licensean Conditions on Wiley Online Library.

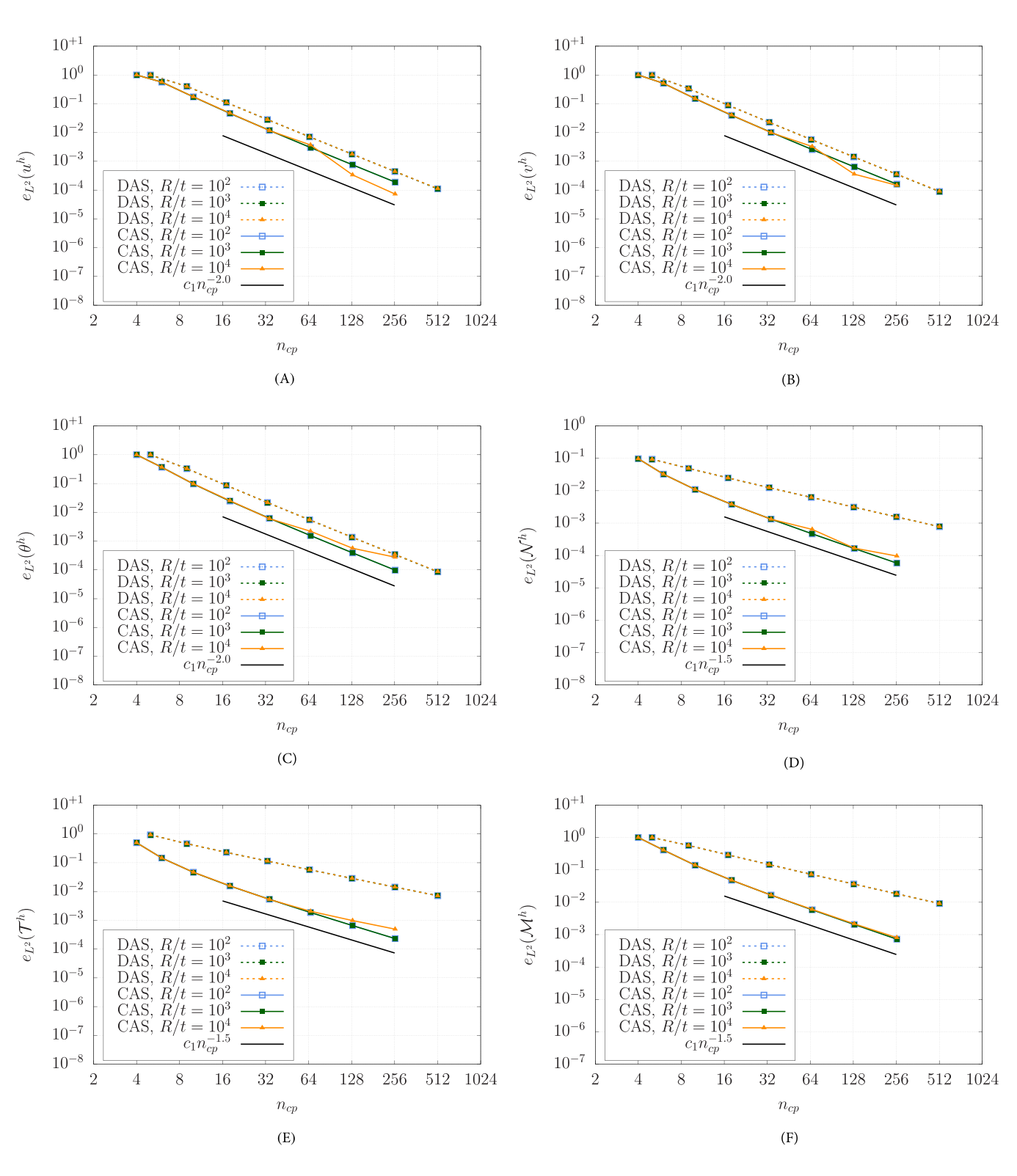


FIGURE 11 (Color online) Clamped-clamped semi-circular arc under a distributed load. Convergence of the (A) tangential and (B) normal displacements, (C) the rotation, (D) the membrane force, (E) the shear force, and (F) the bending moment with respect to the number of control points using DAS elements and CAS elements. Both CAS and DAS elements vanquish locking, but CAS elements result in higher accuracy.

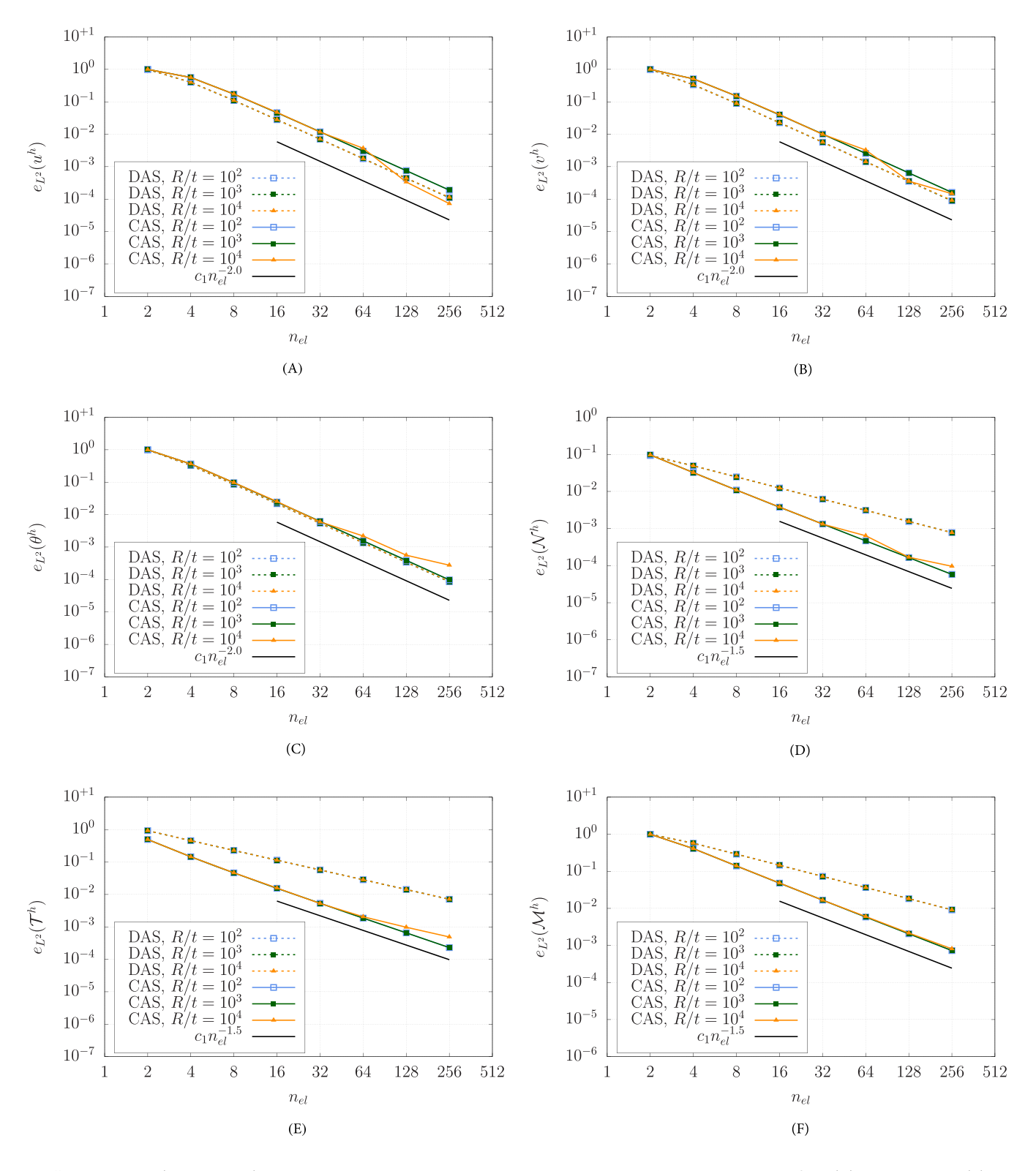


FIGURE 12 (Color online) Clamped-clamped semi-circular arc under a distributed load. Convergence of the (A) tangential and (B) normal displacements, (C) the rotation, (D) the membrane force, (E) the shear force, and (F) the bending moment with respect to the number of elements using DAS elements and CAS elements. Both CAS and DAS elements vanquish locking, but CAS elements result in higher accuracy.

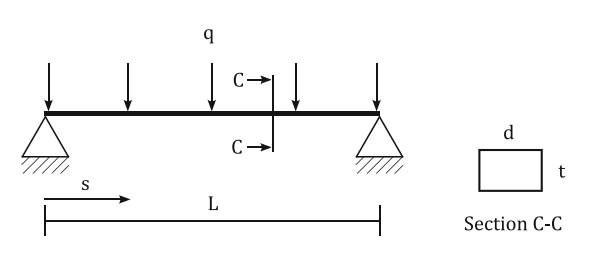


FIGURE 13 Geometry, boundary conditions, and applied load for the simply-supported straight rod under a distributed load.

**TABLE 1** Clamped-clamped semi-circular arc under a distributed load. Condition numbers for NURBS elements, CAS elements, DAS elements, and linear Lagrange polynomials for  $R/t = 10^3$ .

$n_{el}$	FEM	NURBS	CAS	DAS
2	4.277438e+08	3.471324e+08	2.306525e+08	4.559788e+08
4	3.007571e+08	2.894053e+08	2.612427e+08	3.098465e+08
8	4.132764e+08	1.720973e+08	1.652224e+08	4.096552e+08
16	8.480759e+08	3.368758e+08	3.338030e+08	8.489835e+08
32	1.707429e+09	6.833800e+08	6.811998e+08	1.762594e+09
64	3.420561e+09	1.385347e+09	1.383758e+09	3.619738e+09
128	6.843982e+09	2.798342e+09	2.797163e+09	7.956930e+09
256	1.368939e+10	6.119361e+09	6.118801e+09	3.210496e+10

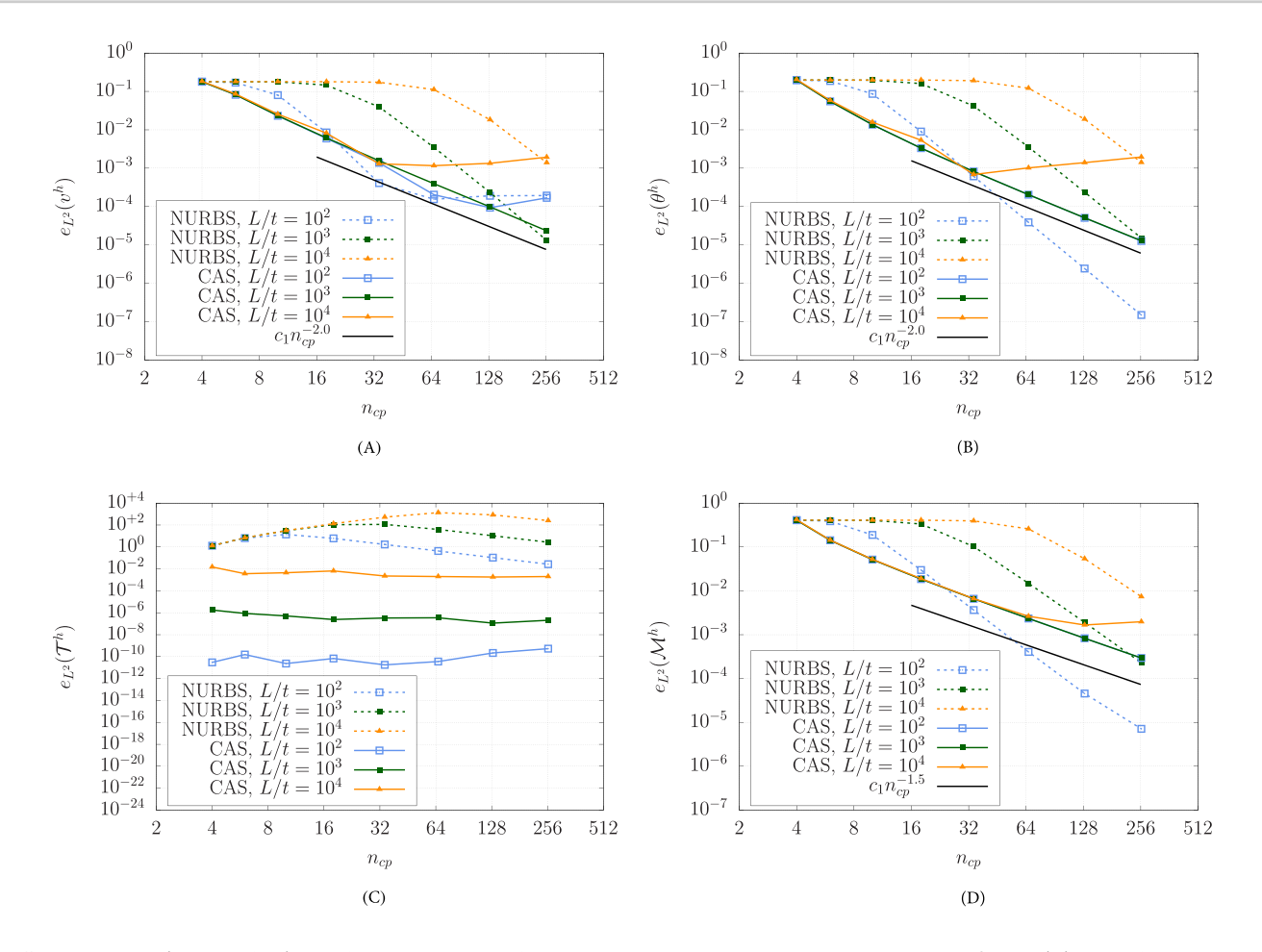
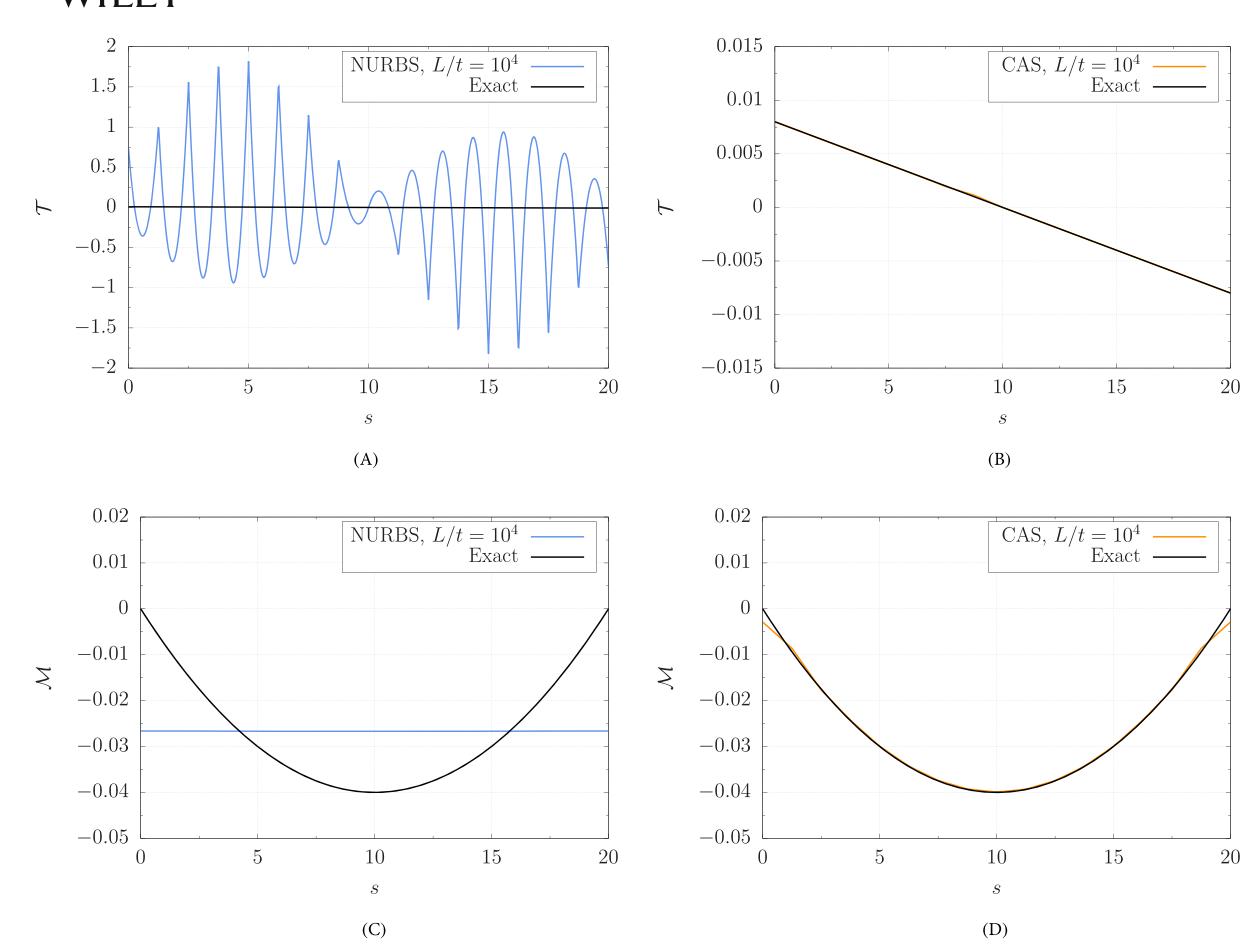


FIGURE 14 (Color online) Simply-supported straight rod under a distributed load. Convergence rate for the (A) normal displacement, (B) the rotation, (C) the shear force, and (D) the bending moment using NURBS elements and CAS elements.



**FIGURE 15** (Color online) Shear force and bending moment of the simply-supported straight rod under a distributed load using (A, C) NURBS and (B, D) CAS elements. The mesh has 16 elements and  $L/t = 10^4$ . The numerical solution of the shear force using CAS elements overlaps with the exact solution. NURBS elements lock resulting in zero bending moment and large-amplitude spurious oscillations of the shear force. Note the different vertical scale used in each plot.

In any case, the accuracy of the stress resultants using CAS elements is high even for the extreme slenderness ratio of  $L/t = 10^4$  as shown in Figure 15. For the same mesh resolution (16 elements) and L/t ratio, NURBS elements result in a flat distribution of the bending moment and large-amplitude spurious oscillations of the shear forces (the absolute value of the maximum shear force obtained with NURBS elements divided by the maximum exact shear force is 227.54) as shown in Figure 15.

We now solve this problem using a simple reduced integration rule with p Gauss points (2GP) to compute all the integrals and conduct comparisons with respect to the full integration rule with p+1 Gauss points (3GP). As shown in Figures 16 and 17, the convergence of NURBS elements gets better when 2 Gauss points are used instead of 3 Gauss points. Nevertheless, the convergence of NURBS elements with 2 Gauss points still worsens significantly as L/t increases. The convergence of the shear force using NURBS elements with 2 Gauss points is completely unsatisfactory (the error even increases as the mesh is refined for multiple refinement levels) since the large-amplitude spurious oscillations of the shear force are still present. For coarse meshes, the accuracy of the normal displacement, the rotation, and the bending moment barely increase when using NURBS elements with 2 Gauss points. This is relevant for complex industrial applications which often require to work with coarse meshes to obtain manageable computational times. On the other hand, CAS elements result in essentially the same accuracy regardless of whether 2 Gauss points or 3 Gauss points are used. Therefore, 2 Gauss points can be used to decrease the computational time when using CAS elements.

As in Section 5.2, we also computed the condition numbers of NURBS elements, CAS elements, and linear Lagrange polynomials for  $R/t = 10^3$ . The values of the condition number are included in Table 2. The trends that are obtained for this example are the same as those obtained in Section 5.2.



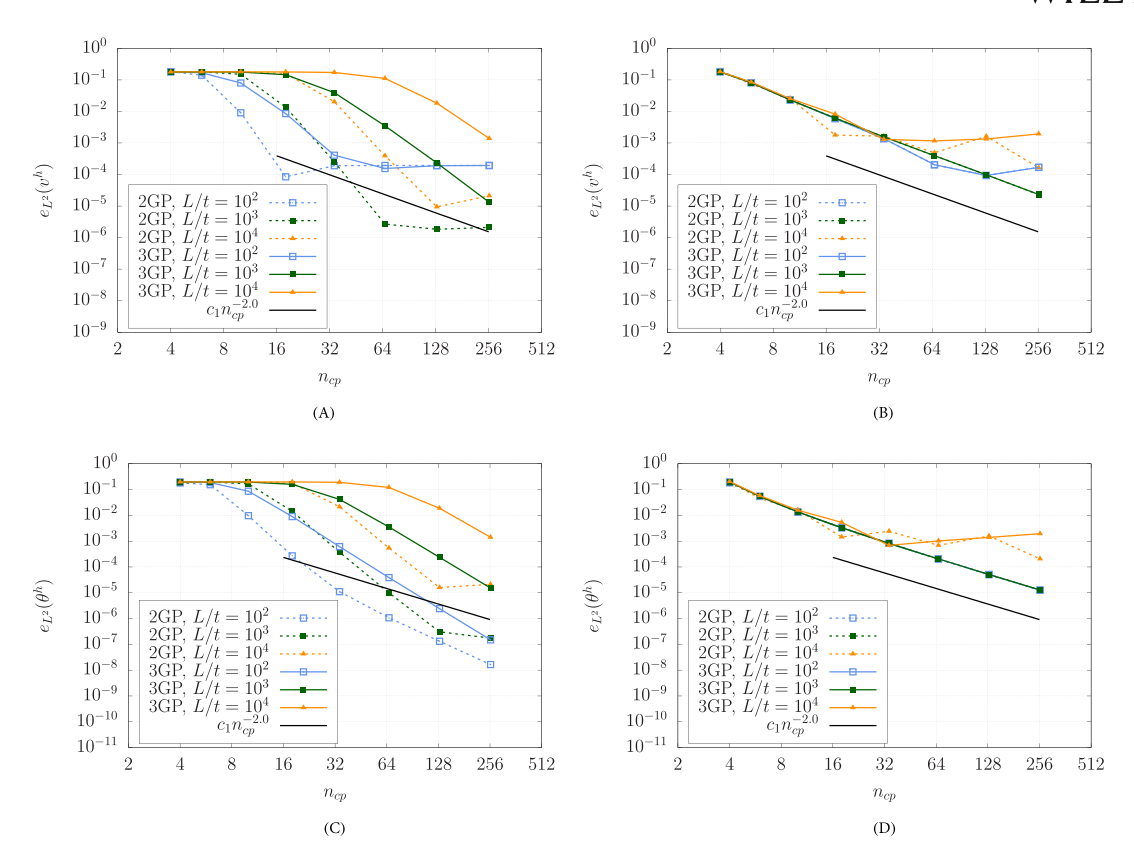


**FIGURE 16** (Color online) Simply-supported straight rod under a distributed load. Convergence comparison of (A, C) NURBS elements and (B, D) CAS elements for the normal displacement and the rotation using either 3 Gauss points or 2 Gauss points.

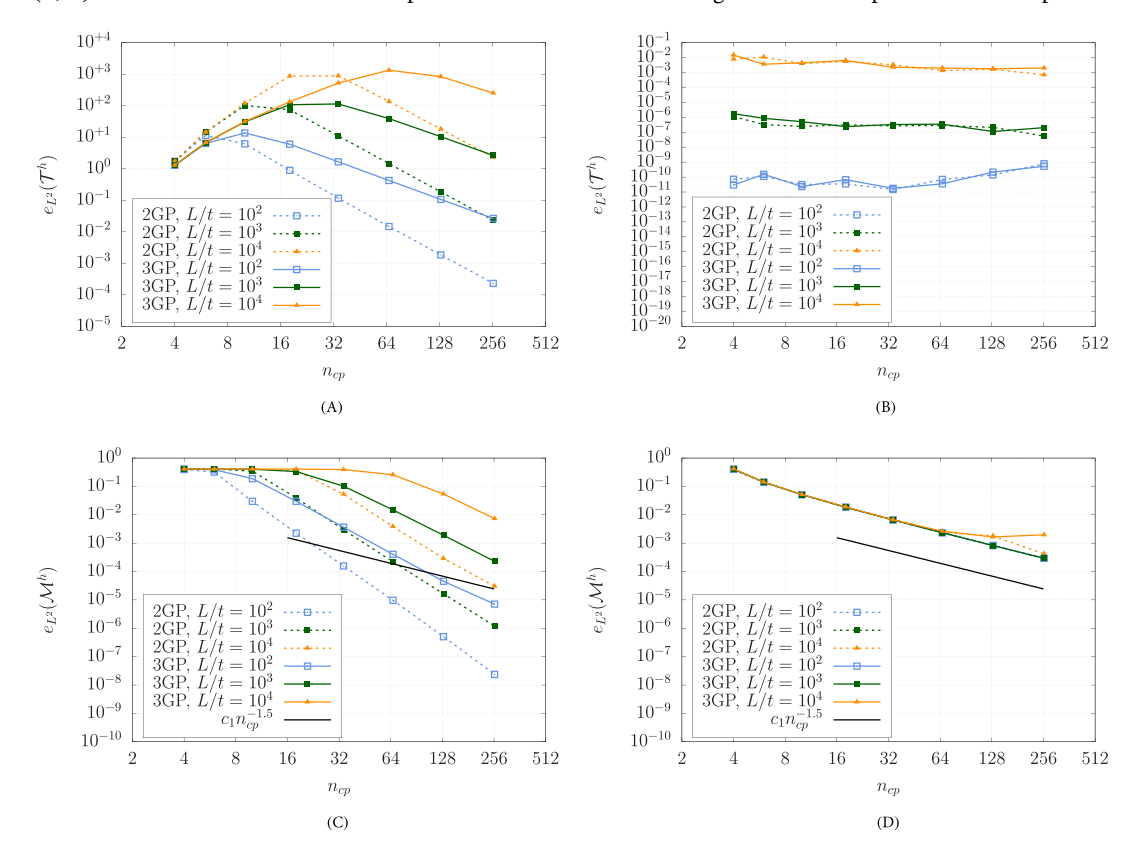


**FIGURE 17** (Color online) Simply-supported straight rod under a distributed load. Convergence comparison of (B, D) NURBS elements and (A, C) CAS elements for the shear force and the bending moment using either 3 Gauss points or 2 Gauss points.

10970207, 0, Downloaded from https://onlinelibrary.wiley.com/doi/10.1002/nme.7257, Wiley Online Library on [28/07/2023]. See the Terms and Conditions (https://onlinelibrary.wiley.com/terms-and-conditions) on Wiley Online Library for rules of use; OA articles are governed by the applicable Creative Commons Licensea (https://onlinelibrary.wiley.com/terms-and-conditions) on Wiley Online Library for rules of use; OA articles are governed by the applicable Creative Commons Licensea (https://onlinelibrary.wiley.com/terms-and-conditions) on Wiley Online Library on [28/07/2023].

**TABLE 2** Simply supported straight rod. Condition numbers for NURBS elements, CAS elements, and linear Lagrange polynomials for  $R/t = 10^3$ .

$n_{el}$	FEM	NURBS	CAS
2	1.293921e+10	9.529486e+09	8.203125e+09
4	7.657799e+09	7.143762e+09	6.574945e+09
8	6.464235e+09	4.028596e+09	3.927086e+09
16	1.331088e+10	5.033083e+09	5.033083e+09
32	2.681528e+10	1.007633e+10	1.007633e+10
64	5.372762e+10	2.015822e+10	2.015822e+10
128	1.075038e+11	4.031910e+10	4.031910e+10
256	2.150319e+11	8.063955e+10	8.063955e+10

# 6 | CONCLUSIONS AND FUTURE WORK

In this work, linear plane curved Timoshenko rods are used as a model problem to investigate how to properly remove shear and membrane locking from quadratic NURBS-based discretizations of structural theories that take into account transverse shear deformations. The numerical investigations of Section 5 show that locking-prone discretizations undergo three separate regimes as the element size is decreased:

- Regime 1: The displacements, the rotation, and the bending moment lock resulting in much smaller values than expected and the shear and membrane forces lock resulting in large-amplitude spurious oscillations.
- Regime 2: The displacements, the rotation, and the bending moment start to unlock and eventually have accurate values while the shear and membrane forces are still locked resulting in large-amplitude spurious oscillations (the amplitude of the spurious oscillations may have even increased in comparison with the oscillations in Regime 1).
- Regime 3: The shear and membrane forces start to unlock and eventually have accurate values while the displacements, the rotation, and the bending moment already have accurate values.

The number of refinement levels that belong to Regimes 1 and 2 increase as the slenderness ratio is increased. As shown in Figures 6 and 14, the number of refinements levels that belong to Regime 2 is high. Therefore, when the effectivity of a locking treatment is evaluated, it is not enough to only study the accuracy of the unknowns (displacements and rotations) since the effectivity of the locking treatment in removing Regime 2 is not evaluated at all. Thus, the authors strongly recommend to always evaluate the effectivity of a locking treatment studying the accuracy of both the unknowns and the stress resultants. The numerical investigations of Section 5 show that CAS elements remove shear and membrane locking for an ample range of slenderness ratios, that is, both Regime 1 and Regime 2 disappear. CAS elements overcome shear and membrane locking by means of interpolating the shear and membrane strains using linear Lagrange polynomials while maintaining the  $C^0$  continuity across elements of the shear and membrane strains. The convergence of the displacements, the rotation, the membrane force, the shear force, and the bending moment is independent of the slenderness ratio up to  $10^4$  using CAS elements. Lastly, for a given mesh, CAS elements are almost as computationally efficient as the locking-prone NURBS-based discretization of the Galerkin method.

Future research directions include:

- Extend CAS elements to the nonlinear regime.
- Generalize CAS elements to remove locking from shell formulations.
- Treat the volumetric locking of nearly incompressible solids using CAS elements.

## **ACKNOWLEDGMENTS**

Hugo Casquero and Mahmoud Golestanian were partially supported by the NSF Grant CMMI-2138187, Honda Motor Co., and Ansys Inc.

## DATA AVAILABILITY STATEMENT

The data that support the findings of this study are available from the corresponding author upon reasonable request.

# **ENDNOTE**

\*Alternatively, accuracy per computational time could be compared directly. However, this type of comparison is not particularly reliable for rod discretizations since the computational times are very small.

## ORCID

Hugo Casquero https://orcid.org/0000-0003-4176-4261

## REFERENCES

- 1. Hughes TJR, Cottrell JA, Bazilevs Y. Isogeometric analysis: CAD, finite elements, NURBS, exact geometry and mesh refinement. Comput Methods Appl Mech Eng. 2005;194:4135-4195.
- 2. Cottrell JA, Hughes TJR, Bazilevs Y. Isogeometric Analysis: Toward Integration of CAD and FEA. John Wiley & Sons; 2009.
- 3. Nagy AP, Abdalla MM, Gürdal Z. Isogeometric sizing and shape optimisation of beam structures. Comput Methods Appl Mech Eng. 2010;199(17-20):1216-1230.
- 4. Greco L, Cuomo M. B-spline interpolation of Kirchhoff-Love space rods. Comput Methods Appl Mech Eng. 2013;256:251-269.
- 5. Kiendl J, Auricchio F, Hughes TJ, Reali A. Single-variable formulations and isogeometric discretizations for shear deformable beams. Comput Methods Appl Mech Eng. 2015;284:988-1004.
- 6. Greco L, Cuomo M. An isogeometric implicit G1 mixed finite element for Kirchhoff space rods. Comput Methods Appl Mech Eng. 2016;298:325-349.
- 7. Bauer A, Breitenberger M, Philipp B, Wüchner R, Bletzinger KU. Nonlinear isogeometric spatial Bernoulli beam. Comput Methods Appl Mech Eng. 2016;303:101-127.
- 8. Tasora A, Benatti S, Mangoni D, Garziera R. A geometrically exact isogeometric beam for large displacements and contacts. Comput Methods Appl Mech Eng. 2020;358:112635.
- 9. Kiendl J, Bletzinger KU, Linhard J, Wuchner R. Isogeometric shell analysis with Kirchhoff-Love elements. Comput Methods Appl Mech Eng. 2009;198:3902-3914.
- 10. Benson D, Bazilevs Y, Hsu M, Hughes TJR. Isogeometric shell analysis: the Reissner-Mindlin shell. Comput Methods Appl Mech Eng. 2010:199:276-289.
- 11. Dornisch W, Klinkel S, Simeon B. Isogeometric Reissner-Mindlin shell analysis with exactly calculated director vectors. Comput Methods Appl Mech Eng. 2013;253:491-504.
- 12. Casquero H, Liu L, Zhang Y, Reali A, Kiendl J, Gomez H. Arbitrary-degree T-splines for isogeometric analysis of fully nonlinear Kirchhoff-Love shells. Comput-Aided Des. 2017;82:140-153.
- 13. Duong TX, Roohbakhshan F, Sauer RA. A new rotation-free isogeometric thin shell formulation and a corresponding continuity constraint for patch boundaries. Comput Methods Appl Mech Eng. 2017;316:43-83.
- 14. Casquero H, Wei X, Toshniwal D, et al. Seamless integration of design and Kirchhoff-love shell analysis using analysis-suitable unstructured T-splines. Comput Methods Appl Mech Eng. 2020;360:112765.
- 15. Liu N, Johnson EL, Rajanna MR, Lua J, Phan N, Hsu MC. Blended isogeometric Kirchhoff-Love and continuum shells. Comput Methods Appl Mech Eng. 2021:385:114005.
- 16. Benzaken J, Evans JA, McCormick SF, Tamstorf R. Nitsche's method for linear Kirchhoff-Love shells: formulation, error analysis, and verification. Comput Methods Appl Mech Eng. 2021;374:113544.
- 17. Wei X, Li X, Qian K, Hughes TJR, Zhang YJ, Casquero H. Analysis-suitable unstructured T-splines: multiple extraordinary points per face. Comput Methods Appl Mech Eng. 2022;391:114494.
- 18. Wen Z, Faruque MS, Li X, Wei X, Casquero H. Isogeometric analysis using G-spline surfaces with arbitrary unstructured quadrilateral layout. Comput Methods Appl Mech Eng. 2023;408:115965.
- 19. Echter R, Bischoff M. Numerical efficiency, locking and unlocking of NURBS finite elements. Comput Methods Appl Mech Eng. 2010;199(5-8):374-382.
- 20. Bieber S, Oesterle B, Ramm E, Bischoff M. A variational method to avoid locking-independent of the discretization scheme. Int J Numer Methods Eng. 2018;114(8):801-827.
- 21. Kikis G, Dornisch W, Klinkel S. Adjusted approximation spaces for the treatment of transverse shear locking in isogeometric Reissner-Mindlin shell analysis. Comput Methods Appl Mech Eng. 2019;354:850-870.
- 22. Bouclier R, Elguedj T, Combescure A. Locking free isogeometric formulations of curved thick beams. Comput Methods Appl Mech Eng. 2012;245:144-162.
- 23. Adam C, Bouabdallah S, Zarroug M, Maitournam H. Improved numerical integration for locking treatment in isogeometric structural elements. Part I: beams. Comput Methods Appl Mech Eng. 2014;279:1-28.
- 24. Hu P, Hu Q, Xia Y. Order reduction method for locking free isogeometric analysis of Timoshenko beams. Comput Methods Appl Mech Eng. 2016:308:1-22.
- 25. Miao D, Borden MJ, Scott MA, Thomas DC. Bézier B projection. Comput Methods Appl Mech Eng. 2018;335:273-297.

- 26. Zhang G, Alberdi R, Khandelwal K. On the locking free isogeometric formulations for 3-D curved Timoshenko beams. Finite Elem Anal Des. 2018:143:46-65.
- 27. Echter R, Oesterle B, Bischoff M. A hierarchic family of isogeometric shell finite elements. Comput Methods Appl Mech Eng. 2013;254:170-180.
- 28. Adam C, Bouabdallah S, Zarroug M, Maitournam H. Improved numerical integration for locking treatment in isogeometric structural elements. Part II: plates and shells. Comput Methods Appl Mech Eng. 2015;284:106-137.
- 29. Zou Z, Hughes TJR, Scott M, Sauer R, Savitha E. Galerkin formulations of isogeometric shell analysis; alleviating locking with Greville quadratures and higher-order elements. Comput Methods Appl Mech Eng. 2021;380:113757.
- 30. Zou Z, Hughes TJR, Scott M, Miao D, Sauer R. Efficient and robust quadratures for isogeometric analysis: reduced Gauss and Gauss-Greville rules. Comput Methods Appl Mech Eng. 2022;392:114722.
- 31. Kikis G, Klinkel S. Two-field formulations for isogeometric Reissner-Mindlin plates and shells with global and local condensation. Comput Mech. 2022:69(1):1-21.
- 32. Zienkiewicz O, Taylor R, Too J. Reduced integration technique in general analysis of plates and shells. Int J Numer Methods Eng. 1971;3(2):275-290.
- 33. Flanagan D, Belytschko T. A uniform strain hexahedron and quadrilateral with orthogonal hourglass control. Int J Numer Methods Eng. 1981;17(5):679-706.
- 34. Belytschko T, Ong JSJ, Liu WK, Kennedy JM. Hourglass control in linear and nonlinear problems. Comput Methods Appl Mech Eng. 1984;43(3):251-276.
- 35. Belytschko T, Lin JI, Chen-Shyh T. Explicit algorithms for the nonlinear dynamics of shells. Comput Methods Appl Mech Eng. 1984;42(2):225-251.
- 36. Hughes TJR, Taylor RL, Kanoknukulchai W. A simple and efficient finite element for plate bending. Int J Numer Methods Eng. 1977;11(10):1529-1543.
- 37. Hughes TJR, Cohen M, Haroun M. Reduced and selective integration techniques in the finite element analysis of plates. Nucl Eng Des. 1978;46(1):203-222.
- 38. Hughes TJR, Liu WK. Nonlinear finite element analysis of shells-part II. Two-dimensional shells. Comput Methods Appl Mech Eng. 1981;27(2):167-181.
- 39. MacNeal RH. A simple quadrilateral shell element. Comput Struct. 1978;8(2):175-183.
- 40. Hughes TJR, Tezduyar T. Finite elements based upon Mindlin plate theory with particular reference to the four-node bilinear isoparametric element. J Appl Mech. 1981;48:587-596.
- 41. Macneal RH. Derivation of element stiffness matrices by assumed strain distributions. Nucl Eng Des. 1982;70(1):3-12.
- 42. Dvorkin EN, Bathe KJ. A continuum mechanics based four-node shell element for general non-linear analysis. Eng Comput. 1984;1:77-88.
- 43. Lee S, Rhiu J. A new efficient approach to the formulation of mixed finite element models for structural analysis. Int J Numer Methods Eng. 1986;23(9):1629-1641.
- 44. Wagner W, Gruttmann F. A robust non-linear mixed hybrid quadrilateral shell element. Int J Numer Methods Eng. 2005;64(5):635-666.
- 45. Klinkel S, Gruttmann F, Wagner W. A mixed shell formulation accounting for thickness strains and finite strain 3D material models. Int J Numer Methods Eng. 2008;74(6):945-970.
- 46. Greco L, Cuomo M, Contrafatto L, Gazzo S. An efficient blended mixed B-spline formulation for removing membrane locking in plane curved Kirchhoff rods. Comput Methods Appl Mech Eng. 2017;324:476-511.
- 47. Greco L, Cuomo M, Contrafatto L. A reconstructed local B formulation for isogeometric Kirchhoff-Love shells. Comput Methods Appl Mech Eng. 2018;332:462-487.
- 48. Bouclier R, Elguedj T, Combescure A. Efficient isogeometric NURBS-based solid-shell elements: mixed formulation and B-method. Comput Methods Appl Mech Eng. 2013;267:86-110.
- 49. Kim MG, Lee GH, Lee H, Koo B. Isogeometric analysis for geometrically exact shell elements using Bézier extraction of NURBS with assumed natural strain method. Thin-Walled Struct. 2022;172:108846.
- 50. Casquero H, Golestanian M. Removing membrane locking in quadratic NURBS-based discretizations of linear plane Kirchhoff rods: CAS elements. Comput Methods Appl Mech Eng. 2022;399:115354.
- 51. Adam C, Hughes TJR, Bouabdallah S, Zarroug M, Maitournam H. Selective and reduced numerical integrations for NURBS-based isogeometric analysis. Comput Methods Appl Mech Eng. 2015;284:732-761.
- 52. Leonetti L, Liguori F, Magisano D, Garcea G. An efficient isogeometric solid-shell formulation for geometrically nonlinear analysis of elastic shells. Comput Methods Appl Mech Eng. 2018;331:159-183.
- 53. Leonetti L, Magisano D, Madeo A, Garcea G, Kiendl J, Reali A. A simplified Kirchhoff-Love large deformation model for elastic shells and its effective isogeometric formulation. Comput Methods Appl Mech Eng. 2019;354:369-396.
- 54. Zou Z, Scott MA, Miao D, Bischoff M, Oesterle B, Dornisch W. An isogeometric Reissner-Mindlin shell element based on Bézier dual basis functions: overcoming locking and improved coarse mesh accuracy. Comput Methods Appl Mech Eng. 2020;370:113283.
- 55. Zou Z, Scott MA, Borden MJ, Thomas DC, Dornisch W, Brivadis E. Isogeometric Bézier dual mortaring: Refineable higher-order spline dual bases and weakly continuous geometry. Comput Methods Appl Mech Eng. 2018;333:497-534.
- 56. Miao D, Zou Z, Scott MA, Borden MJ, Thomas DC. Isogeometric Bézier dual mortaring: the enriched Bézier dual basis with application to second-and fourth-order problems. Comput Methods Appl Mech Eng. 2020;363:112900.
- 57. Simo JC, Hughes TJR. On the variational foundations of assumed strain methods. J Appl Mech. 1986;53(1):51-54.

- 58. Elguedj T, Bazilevs Y, Calo VM, Hughes TJR. Over(B, -) and over(F, -) projection methods for nearly incompressible linear and non-linear elasticity and plasticity using higher-order NURBS elements. *Comput Methods Appl Mech Eng.* 2008;197:2732-2762.
- 59. Bletzinger KU, Bischoff M, Ramm E. A unified approach for shear-locking-free triangular and rectangular shell finite elements. *Comput Struct*. 2000;75(3):321-334.
- 60. Koschnick F, Bischoff M, Camprubí N, Bletzinger KU. The discrete strain gap method and membrane locking. *Comput Methods Appl Mech Eng.* 2005;194(21-24):2444-2463.
- 61. Piegl L, Tiller W. The NURBS Book. Springer Science & Business Media; 2012.
- 62. Hughes TJR. The Finite Element Method: Linear Static and Dynamic Finite Element Analysis. Courier Corporation; 2012.
- 63. Dalcin L, Collier N, Vignal P, Côrtes A, Calo VM. PetIGA: a framework for high-performance isogeometric analysis. *Comput Methods Appl Mech Eng.* 2016;308:151-181.
- 64. Balay S, Adams MF, Brown J, et al. PETSc Web page; 2014. http://www.mcs.anl.gov/petsc
- 65. Cazzani A, Malagù M, Turco E. Isogeometric analysis of plane-curved beams. Math Mech Solids. 2016;21(5):562-577.

**How to cite this article:** Golestanian M, Casquero H. Extending CAS elements to remove shear and membrane locking from quadratic NURBS-based discretizations of linear plane Timoshenko rods. *Int J Numer Methods Eng.* 2023;1-25. doi: 10.1002/nme.7257